


Planar cell polarity gene *Fuz* triggers apoptosis in neurodegenerative disease models

Zhefan Stephen Chen^{1,2}, Li Li^{1,2}, Shaohong Peng^{1,2}, Francis M Chen³, Qian Zhang^{1,2}, Ying An^{1,2}, Xiao Lin², Wen Li², Alex Chun Koon^{1,2}, Ting-Fung Chan^{2,3,4,5}, Kwok-Fai Lau^{2,3,4}, Jacky Chi Ki Ngo^{2,3}, Wing Tak Wong³, Kin Ming Kwan^{3,6,7} & Ho Yin Edwin Chan^{1,2,3,4,5,*} 

Abstract

Planar cell polarity (PCP) describes a cell–cell communication process through which individual cells coordinate and align within the plane of a tissue. In this study, we show that overexpression of *Fuz*, a PCP gene, triggers neuronal apoptosis via the dishevelled/Rac1 GTPase/MEKK1/JNK/caspase signalling axis. Consistent with this finding, endogenous *Fuz* expression is upregulated in models of polyglutamine (polyQ) diseases and in fibroblasts from spinocerebellar ataxia type 3 (SCA3) patients. The disruption of this upregulation mitigates polyQ-induced neurodegeneration in *Drosophila*. We show that the transcriptional regulator Yin Yang 1 (YY1) associates with the *Fuz* promoter. Overexpression of YY1 promotes the hypermethylation of *Fuz* promoter, causing transcriptional repression of *Fuz*. Remarkably, YY1 protein is recruited to ATXN3-Q84 aggregates, which reduces the level of functional, soluble YY1, resulting in *Fuz* transcriptional derepression and induction of neuronal apoptosis. Furthermore, *Fuz* transcript level is elevated in amyloid beta-peptide, Tau and α -synuclein models, implicating its potential involvement in other neurodegenerative diseases, such as Alzheimer's and Parkinson's diseases. Taken together, this study unveils a generic *Fuz*-mediated apoptotic cell death pathway in neurodegenerative disorders.

Keywords alpha-synuclein; amyloid beta-peptide; polyglutamine; Tau; Yin Yang 1

Subject Categories Autophagy & Cell Death; Neuroscience

DOI 10.15252/embr.201745409 | Received 31 October 2017 | Revised 15 June 2018 | Accepted 22 June 2018 | Published online 19 July 2018

EMBO Reports (2018) 19: e45409

Introduction

Planar cell polarity (PCP) signalling is an evolutionarily conserved pathway by which directional information regarding polarized cell movement, e.g., along an epithelial plane, is provided to cells [1]. The PCP signalling axis involves two subsets of genes, PCP core and PCP effector genes. Once stimulated, the core and effector genes are activated consecutively to govern orientated cell migration and the establishment of cytoskeletal structures [1]. *Dishevelled* (*Dvl* in mammals or *Dsh* in *Drosophila* [2]) and *Fuz* (or *fuzzy* in *Drosophila* [3]) are two representative PCP core and effector genes, respectively [4]. It has been reported that PCP regulates mammalian nervous system development. In mice, the disruption of *Dvl* function causes hydrocephalus [5] and that a *Fuz*-null mutant displays neural tube defects (NTDs) [6]. Dominant mutations in *Fuz* were reported to cause NTDs in humans [7]. A functional study of these dominant mutations revealed a failure of directional cell motility and cell fusion, supporting that *Fuz* mutants perturb the closure of neural tubes [7]. These observations suggest *Fuz* is essential for the development of the human nervous system. However, whether *Fuz* plays a role in neurodegenerative diseases is unclear.

Polyglutamine (polyQ) diseases, including Huntington's disease and several types of spinocerebellar ataxias, encompass a set of neurodegenerative disorders [8]. These diseases are caused by the expansion of CAG repeats, which code for glutamines, in the open reading frames of the affected genes [9]. The clinical features presented by polyQ patients include loss of movement coordination and cognitive disabilities [10,11]. Perturbation of various molecular and cellular processes is implicated in the pathology of polyQ diseases including the regulation of apoptosis and gene transcription [12]. Normally, apoptosis is tightly controlled by the expression of anti-apoptotic and pro-apoptotic genes [13]. In polyQ diseases, the misexpression of apoptotic gene triggers the induction of apoptosis, which may contribute to the pathogenesis of the diseases [14,15]. In particular, the caspase cascade has been shown to be activated in

1 Laboratory of *Drosophila* Research, School of Life Sciences, Faculty of Science, The Chinese University of Hong Kong, Shatin, N.T., Hong Kong SAR, China

2 Biochemistry Program, School of Life Sciences, Faculty of Science, The Chinese University of Hong Kong, Shatin, N.T., Hong Kong SAR, China

3 Cell and Molecular Biology Program, School of Life Sciences, Faculty of Science, The Chinese University of Hong Kong, Shatin, N.T., Hong Kong SAR, China

4 Molecular Biotechnology Program, School of Life Sciences, Faculty of Science, The Chinese University of Hong Kong, Shatin, N.T., Hong Kong SAR, China

5 Gerald Choa Neuroscience Centre, The Chinese University of Hong Kong, Shatin, N.T., Hong Kong SAR, China

6 Partner State Key Laboratory of Agrobiotechnology (CUHK), The Chinese University of Hong Kong, Shatin, N.T., Hong Kong SAR, China

7 Centre for Cell and Developmental Biology, The Chinese University of Hong Kong, Shatin, N.T., Hong Kong SAR, China

*Corresponding author. Tel: +852 3943 4021; Fax: +852 2603 7732; E-mail: hyechan@cuhk.edu.hk

polyQ-mediated apoptosis [16,17]. Cleavage of caspases was observed in polyQ patients [18]. In addition to polyQ diseases, apoptosis is also involved in other neurodegenerative diseases including Alzheimer's disease (AD), Tauopathy and Parkinson's disease (PD) [19,20].

Fuz^{-/-} mutant mice were previously reported to display an enhanced rate of cell proliferation [21], implying a role of *Fuz* in maintaining the balance between cell proliferation and cell death. In the current study, we report that overexpression of *Fuz* triggers neuronal apoptosis, and further demonstrate *Fuz* exploits the Dvl-Rac1-MAPK-caspase signalling axis to initiate apoptotic cell death. We demonstrate that the expression of *Fuz/Fuz* is upregulated in polyQ diseases, and the perturbation of *Fuz* expression suppresses neurodegeneration. Furthermore, we show that the transcriptional regulator Yin Yang 1 (YY1) negatively regulates *Fuz* expression via hypermethylating *Fuz* promoter. In polyQ diseases, soluble YY1 protein expression is reduced in patient brains, resulting in hypomethylation of the *Fuz* promoter. Overexpression of YY1 corrects the *Fuz* promoter hypomethylation, reduces the upregulation of *Fuz* and suppresses apoptosis in polyQ disease models. Most importantly, we demonstrate that *Fuz* promoter hypomethylation is a common feature shared by several neurodegenerative conditions that associate with amyloid beta-peptide, Tau and α -synuclein. Our findings indicate *Fuz* functions as a communal pro-apoptotic switch in neurodegenerative diseases.

Results

Fuz stimulates the Dvl/Rac1 GTPase/MEKK1/JNK/caspase signalling pathway to trigger apoptosis

We performed a quantitative real-time polymerase chain reaction (qRT-PCR) analysis to determine the endogenous expression level of *Fuz* in different human tissues. *Fuz* transcript was detected in the normal human brain, kidney and muscle, indicating endogenous

functions of *Fuz* in these organs (Fig EV1A). Within the human brain, endogenous *Fuz* expression was detected in the caudate, substantia nigra and the cerebellar regions (Fig EV1B). To investigate the effect of *Fuz* overexpression, we transfected rat primary cortical neurons with increasing amounts of *flag-Fuz* expression construct (from 0.2 to 1.0 μ g). When the relative level of the overexpressed *Fuz* protein in neurons reached approximately 2.5-folds of the endogenous *Fuz* protein, we detected caspase-3 cleavage (Fig 1A), as well as a significant elevation of neuronal cell death in these neurons (Fig 1B). This indicates that a 2.5-fold elevation of *Fuz* protein in neurons is sufficient to induce noticeable cell death (Fig 1A and B). We thus used this transfection condition to further elucidate the apoptotic signalling pathway mediated by *Fuz*. When *Fuz* was overexpressed in human embryonic kidney (HEK) 293 cells, we also observed a similar cytotoxic effect (Fig 1C). We further showed that *Fuz* overexpression induced cell death through the induction of apoptosis (Fig 1D and E). In contrast, overexpression of other PCP effector (Inturned or Fritz) and core (Dvl or Flamingo) proteins did not induce neuronal cell death (Fig EV1C).

The mitogen-activated protein kinase kinase kinase 1 (MEKK1) was reported to activate apoptosis via the c-Jun N-terminal kinase (JNK) pathway [22]. We observed that *Fuz* overexpression induced the phosphorylation of MEKK1 and JNK, as well as caspase-3 cleavage (Fig 1F). Further, we found that caspase-3 cleavage in *Fuz*-expressing cells was blocked upon the treatment of either the JNK inhibitor SP600125 (Fig 1G) or *MEKK1*-siRNA (Fig 1H). The above results demonstrate that *Fuz* induces apoptosis via the MEKK1/JNK/caspase pathway. Next, we showed that *Fuz* overexpression triggered activation of the Rac family small GTPase 1 (Rac1; Fig 1I). Further, the coexpression of a dominant-negative form of Rac1 (Rac1^{T17N}) diminished *Fuz*-mediated MEKK1/JNK phosphorylation and caspase-3 cleavage (Fig 1J). The activity of small GTPases is regulated by guanine nucleotide exchange factors (GEFs; [23]). T-cell lymphoma invasion and metastasis 1 (*Tiam1*) is a specific GEF for Rac1, and it controls Rac1 activation in neurons [24]. When *Tiam1* expression was knocked down, we found that *Fuz*-induced

Figure 1. Fuz triggers apoptosis via the Dvl-Rac1-MAPK-caspase signalling axis.

- A When overexpressed, *Fuz* induced caspase-3 cleavage in rat primary cortical neurons. Right panel shows the relative fold increase of protein level of *flag-Fuz* to endogenous *Fuz* expressed in transfected neurons. Error bars represent s.e.m., $n = 3$.
- B *Fuz* overexpression caused cell death in rat primary cortical neurons. Error bars represent s.e.m., $n = 3$. Statistical analysis was performed using two-tailed unpaired Student's *t*-test. $**P < 0.01$.
- C *Fuz* overexpression induced cell death in HEK293 cells. Error bars represent s.e.m., $n = 3$. Statistical analysis was performed using two-tailed unpaired Student's *t*-test. $***P < 0.001$.
- D Overexpression of *Fuz* in HEK293 cells triggered apoptosis. TUNEL-positive cells (green) were stained with anti-BrdU antibody, and overexpressed *Fuz* (red) was detected with anti-*flag* antibody. Cell nuclei (blue) were stained with Hoechst 33342. Scale bars: 10 μ m. Right panel shows the quantification of TUNEL assay results. The apoptotic index is calculated by dividing the percentage of TUNEL-positive cells in *empty vector*-transfected or *flag-Fuz*-transfected cells by the percentage of TUNEL-positive cells in the untransfected control. Error bars represent s.e.m., $n = 3$. For every control or experimental group, at least 120 cells were counted in each replicate. Statistical analysis was performed using two-tailed unpaired Student's *t*-test. $*P < 0.05$.
- E *Fuz*-induced cell death was suppressed when the activities of caspases were inhibited in HEK293 cells. Error bars represent s.e.m., $n = 3$. Statistical analysis was performed using one-way ANOVA followed by *post hoc* Tukey's test. $**P < 0.01$, $***P < 0.001$.
- F Overexpression of *Fuz* induced MEKK1 and JNK phosphorylation, as well as caspase-3 cleavage in HEK293 cells. $n = 3$.
- G *Fuz*-induced caspase-3 activation was suppressed by JNK inhibitor SP600125 in HEK293 cells. $n = 3$.
- H Knockdown of *MEKK1* expression suppressed the JNK activation and caspase-3 cleavage in *flag-Fuz*-transfected HEK293 cells. $n = 3$.
- I Overexpression of *Fuz* induced Rac1 activation in HEK293 cells. $n = 3$.
- J Blockage of Rac1 activity using the dominant-negative Rac1^{T17N} mutant protein suppressed the MAPK-caspase pathway activation in *flag-Fuz*-transfected HEK293 cells. $n = 3$.
- K Knockdown of *Dvl* expression suppressed the MAPK-caspase activation in *Fuz*-expressing HEK293 cells. $n = 3$.

Data information: Beta-tubulin was used as loading control. n represents the number of biological replicates. Only representative images and blots are shown. Source data are available online for this figure.

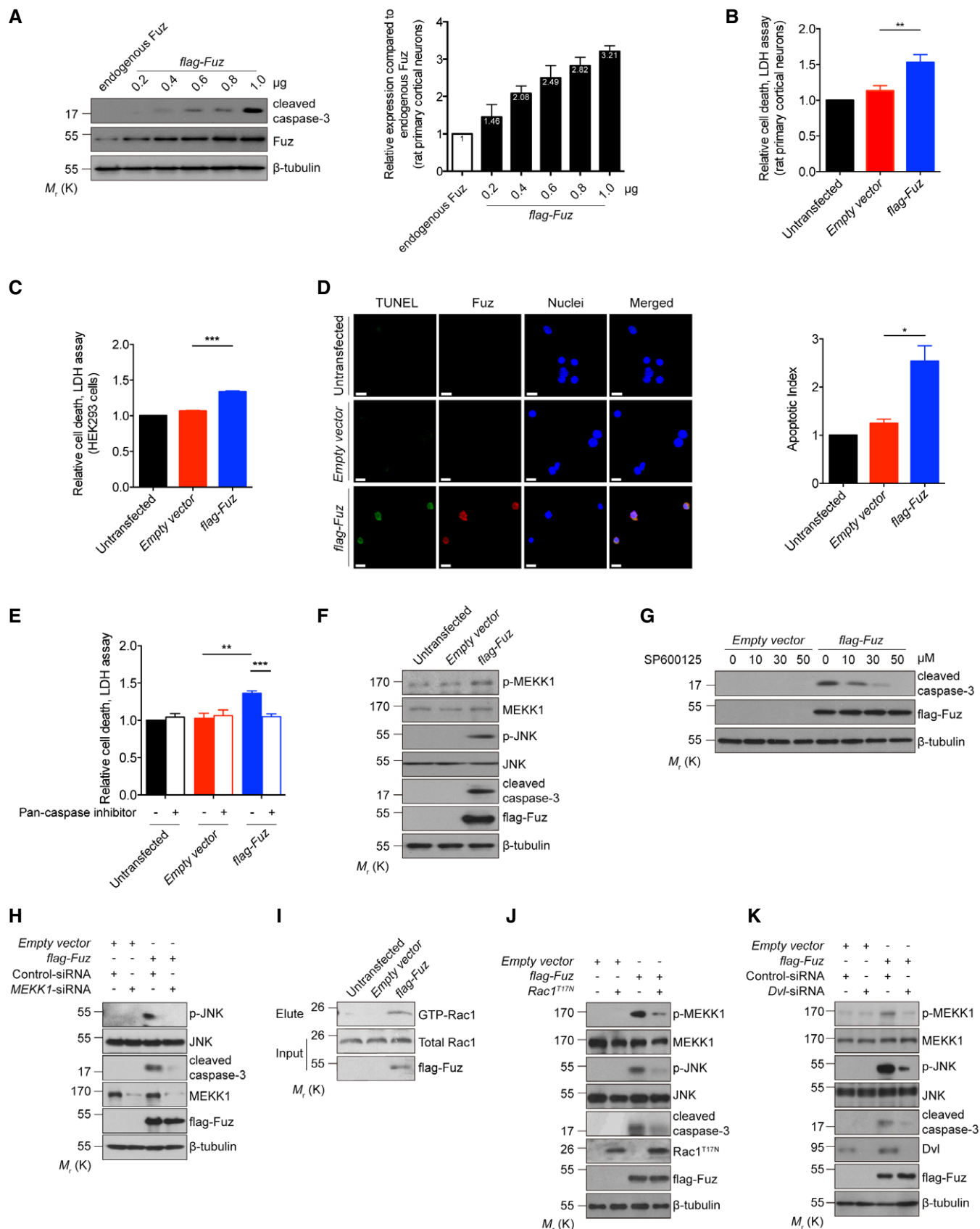


Figure 1.

MEKK1/JNK phosphorylation and caspase-3 cleavage were diminished (Fig EV1D). These results thus highlight the significance of Rac1 and Tiam1 in the Fuz-induced apoptosis pathway.

Fuz interacts with another PCP pathway protein Dvl [25]. Previous studies demonstrated that Dvl “punctae” recruit Rac1 and Tiam1 to a multimeric protein complex for Rac1 activation [26]. We investigated whether Dvl is involved in Fuz-mediated apoptosis. When Dvl was overexpressed alone, 35% of *Dvl*-transfected cells were found to display the Dvl “punctae” pattern (Fig EV1E and F). Upon Fuz coexpression, the percentage of *Dvl/Fuz* double-transfected cell that showed Dvl “punctae” pattern was significantly elevated to 68% (Fig EV1E and F). When Dvl was overexpressed in *Fuz* knockout cells (*Fuz*^{-/-}; Appendix Fig S1A), the percentage of cells that showed Dvl “punctae” pattern was significantly reduced (Fig EV1G). In addition, we observed that Fuz colocalized with Dvl “punctae” in cells and further showed that Fuz and Dvl proteins physically interacted with each other (Fig EV1H). When we knocked down *Dvl* expression in Fuz-expressing cells, a reduction in levels of MEKK1 and JNK phosphorylation, as well as caspase-3 cleavage (Fig 1K), was observed. In contrast, knockdown of the expression of other PCP genes, including *Intumed*, *Fritz* and *Flamingo*, did not affect Fuz-induced caspase-3 cleavage (Fig EV1I–K). Taken together, our findings depict a signalling axis that involves Dvl, Rac1, MEKK1, JNK and the caspase cascade, through which Fuz mediates apoptotic initiation.

Expression of Fuz/Fuz is upregulated in polyglutamine diseases

Given the tissue distribution of *Fuz* in human brain (Fig EV1A) and its pro-apoptotic function (Fig 1A–K), we investigated the role of Fuz in neurodegeneration. Apoptosis is involved in numerous neurodegenerative diseases, including polyglutamine (polyQ) diseases such as Huntington’s disease (HD) and spinocerebellar ataxia type 3 (SCA3). Intriguingly, the induction of *Fuz/Fuz* at both mRNA and protein levels were observed in cell models of HD and SCA3 (Fig EV2A and B). A similar induction was further observed in transgenic *Drosophila* (Fig 2A) and mouse (Fig 2B) models of SCA3, as well as in SCA3 patient fibroblasts (Fig EV2C). We then generated induced neural progenitor cells (iNPCs) from SCA3 patient fibroblasts (Fig EV2D and E) and examined *Fuz* expression in iNPCs. Compared with the control iNPCs, *Fuz/Fuz* expression was elevated in SCA3 iNPCs (Fig 2C). *Fuz* induction was further detected in RNA samples from SCA3 patient brains (Fig 2D). In summary, we observed the upregulation of *Fuz/Fuz* expression in polyQ diseases.

Downregulation of Fuz/fuzzy rescues the cytotoxicity and neurodegeneration in polyQ diseases

Next, we perturbed endogenous *Fuz* expression in our polyQ disease models and examined its effect on apoptosis and neurodegeneration. In contrast to the parental cells, when the SCA3 mutant construct *ATXN3tr-Q78* was expressed in *Fuz*^{-/-} cells (Appendix Fig S1A), we observed a reduction in cell death (Fig 3A), JNK phosphorylation and caspase-3 cleavage (Fig 3B). A similar effect was observed in rat primary cortical neurons transfected with the *ATXN3tr-Q78* transgene (Fig 3C and Appendix Fig S1B), as well as in SCA3 patient fibroblasts (Fig 3D and Appendix Fig S1C) with *Fuz* expression knocked down. These

findings clearly demonstrate the involvement of *Fuz* in ATXN3tr-Q78-induced cell death.

We next knocked down *fuzzy* (*fy*; Appendix Fig S1D), the orthologue of *Fuz*, in *Drosophila* to study its role in polyQ neurodegeneration *in vivo*. When expressed in the *Drosophila* brain, including the retinal neurons, the human disease transgene *ATXN3fl-Q84* induced neurodegeneration ([27]; Fig 3E and F). Both knockdown and knockout of *fy* significantly suppressed the ATXN3fl-Q84-mediated neurodegenerative phenotype (Fig 3E and F, and Appendix Fig S1D–F). In addition, we found that *fy* knockdown mitigated neurodegeneration in a *Drosophila* model of HD (Appendix Fig S1G and H). Taken together, these findings highlight the key role of Fuz in SCA3 pathogenesis, as well as in other polyQ degenerative disorder.

YY1 represses Fuz transcription via hypermethylating Fuz promoter

We next studied the mechanism through which expanded polyQ disease protein induces *Fuz* transcription. We first employed the luciferase assay to define the polyQ-responsive element within the *Fuz* promoter (*Fuz*^{-1332/+574}; Fig EV3A) and found that the *Fuz*^{+68/+574} region responded to expanded polyQ protein expression (Fig EV3A). A YY1 binding site (AATGGG) was predicted within the *Fuz*^{+68/+574} promoter region (Fig 4A), and this binding site is highly conserved among the mammalian genomes (Fig EV3B). YY1 is a multi-functional transcriptional regulator that controls gene expression in the mammalian brain [28], and it plays crucial role in governing neuronal functions [29]. In addition to the predicted YY1 binding site in the *Fuz* promoter, a binding site (ATGGC; [30]) for Pleiohomeotic (PHO), the *Drosophila* orthologue of YY1 [31], was also predicted in the *Drosophila fy* promoter sequence, suggesting that the transcriptional regulation of *Fuz/fy* by YY1/PHO is evolutionarily conserved. Using chromatin immunoprecipitation, we confirmed the binding of YY1 protein to the *Fuz* promoter (*Fuz*^{+117/+347CpG}; Fig 4B) and detected an interaction between YY1 protein and *Fuz* promoter using *in vitro* DNA binding assay (Fig 4C). Our results thus indicate YY1 plays a regulatory role in controlling *Fuz* transcription.

Previous reports illustrate that YY1 can both serve as a transcriptional activator [32] or a repressor [33]. We found that altering one conserved nucleotide in the YY1 binding site in the *Fuz*^{+117/+347CpG} region, from AATGGG to AACGGG, resulted in a significant reduction of the binding of YY1 protein to *Fuz* promoter (Fig 4C and D). When a *Fuz*^{-1332/+574} promoter reporter construct harbouring the same single point mutation was used in a luciferase assay, cells transfected with this mutant (*Fuz*^{-1332/+574} mutant) reporter construct exhibited a 1.9-fold increase of luciferase activity when compared to those expressing the wild-type (*Fuz*^{-1332/+574} wild-type) luciferase construct (Fig 4E). Furthermore, we found that knockdown of YY1 expression led to an increase in endogenous *Fuz/Fuz* expression (Figs 5A and EV3C). In contrast, YY1 overexpression resulted in a downregulation of *Fuz* expression (Fig 5B). These findings indicate that YY1 acts as a transcriptional repressor to attenuate *Fuz* transcription.

Previous studies showed that YY1 mediates gene silencing by recruiting DNA methyltransferase (DNMT) to gene promoters, thus promoting the hypermethylation of CpG islands [34]. We found putative CpG islands (*Fuz*^{+117/+347CpG}; Fig EV3D) within the *Fuz*

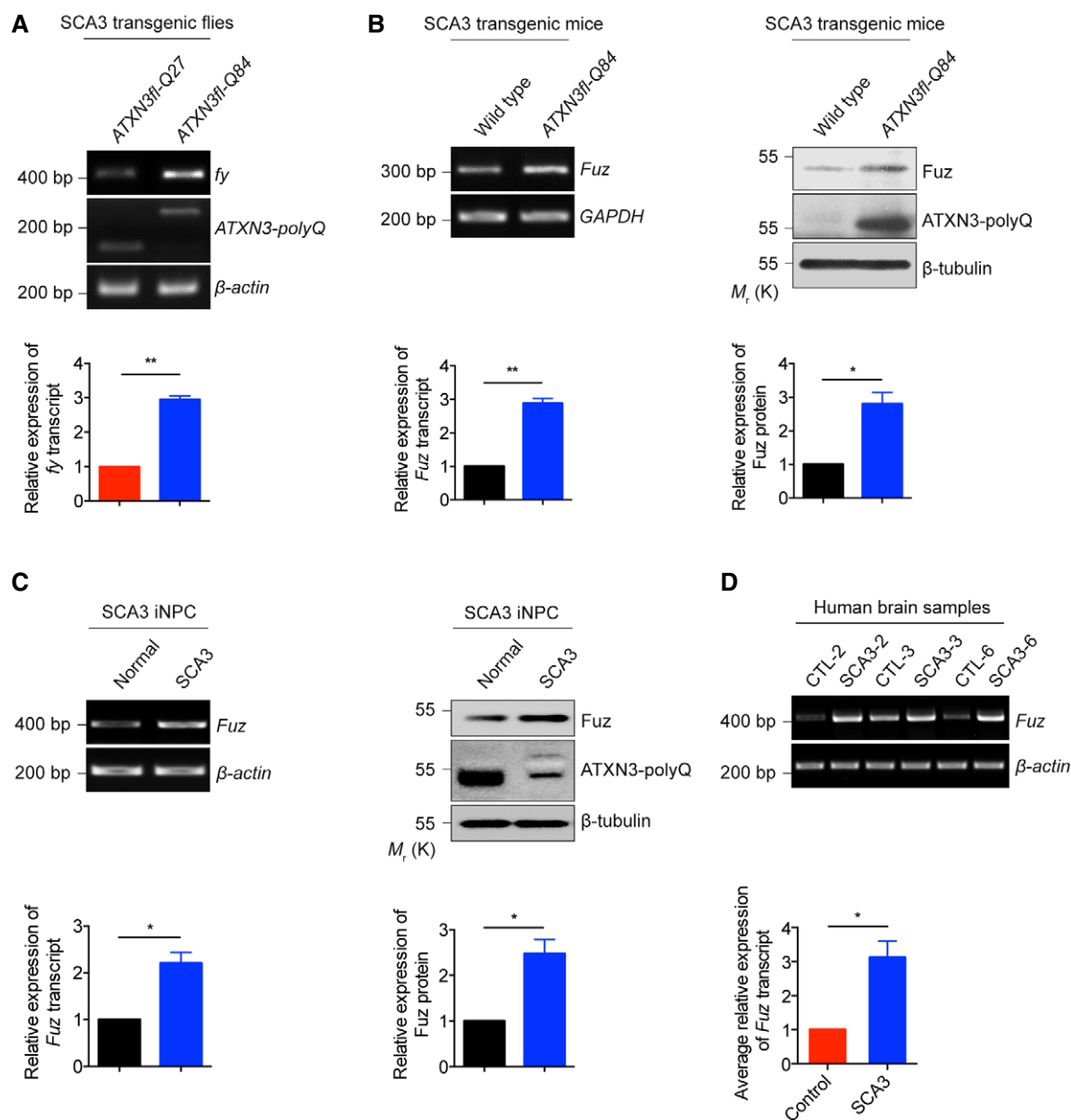


Figure 2. *fuzzy/Fuz* transcription is induced in polyQ diseases.

- A Upregulation of *fy* transcription was observed in a SCA3 transgenic *Drosophila* model. "ATXN3^{fl}" indicates full-length ataxin-3 (ATXN3), disease protein of SCA3. The flies were of genotypes *w; Gmr::Gal4 UAS::ATXN3^{fl}-Q27/+; +/+* and *w; Gmr::Gal4/+; UAS::ATXN3^{fl}-Q84/+*. Lower panel shows the quantification of *fy* transcript expression relative to controls. Error bars represent s.e.m., $n = 3$. Statistical analysis was performed using two-tailed unpaired Student's *t*-test. $**P < 0.01$.
- B The expression levels of *Fuz* transcript and Fuz protein were upregulated in brain samples of 6-month-old SCA3 transgenic mice. Lower panel shows the quantification of *Fuz* transcript and protein expression relative to controls. Error bars represent s.e.m., $n = 3$. Statistical analysis was performed using two-tailed unpaired Student's *t*-test. $*P < 0.05$, $**P < 0.01$.
- C The expression levels of *Fuz* transcript and Fuz protein were upregulated in SCA3 iNPCs. Lower panel shows the quantification of *Fuz* transcript and protein expression relative to controls. Error bars represent s.e.m., $n = 3$. Statistical analysis was performed using two-tailed unpaired Student's *t*-test. $*P < 0.05$.
- D The expression level of *Fuz* transcript was upregulated in SCA3 patient brain samples. Background information on the control and patient brains are summarized in Appendix Table S2. Lower panel shows the quantification of *Fuz* transcript expression relative to controls. Error bars represent s.e.m., $n = 3$. Statistical analysis was performed using two-tailed unpaired Student's *t*-test. $*P < 0.05$.

Data information: *beta-actin*, *GAPDH* or *beta-tubulin* was used as loading control. n represents the number of biological replicates. Only representative gels and blots are shown.

Source data are available online for this figure.

promoter region where the YY1 binding site resides (Fig 4A). To determine whether promoter DNA methylation affects *Fuz* transcriptional control, we treated HEK293 cells with the DNMT inhibitor

5-azacytidine. Upon treatment, we observed an upregulation of *Fuz* expression (Fig 5C). We further demonstrated that YY1 overexpression induced the hypermethylation of the *Fuz*^{+117/+347CpG} (Fig 5D),

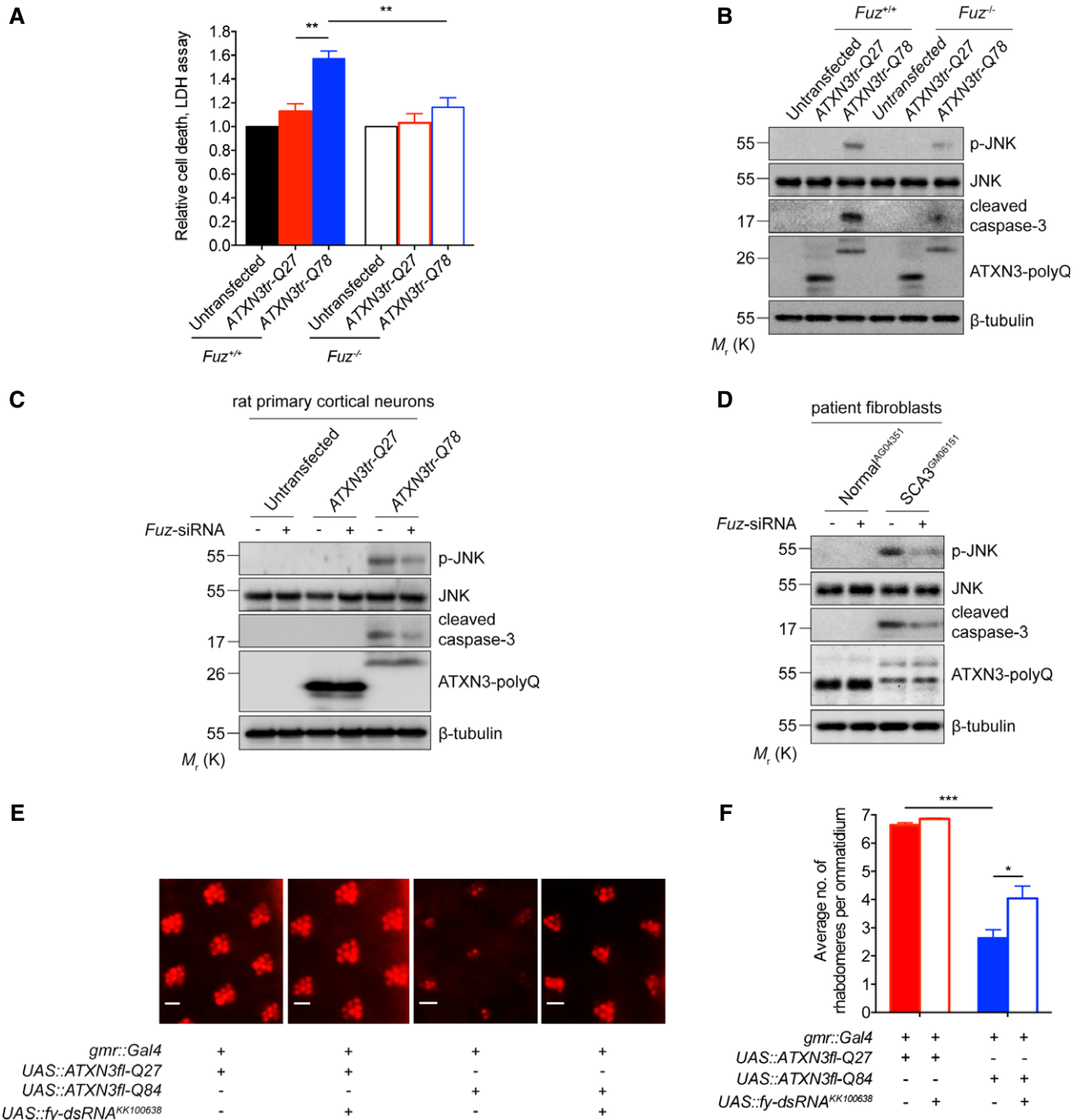


Figure 3. Perturbation of Fuz/fuzzy expression rescues polyQ disease toxicity.

- A** Expression of ATXN3tr-Q78 in *Fuz*^{-/-} HEK293 cells showed reduced cell death. The parental HEK293 cells were used as control. Knockout of *Fuz* did not alter relative cell death in the untransfected or ATXN3tr-Q27 cells, indicating that *Fuz* knockout did not induce cell death. Error bars represent s.e.m., *n* = 3. Statistical analysis was performed using one-way ANOVA followed by *post hoc* Tukey's test. *******P* < 0.01.
- B** The JNK phosphorylation and caspase-3 cleavage induced by ATXN3tr-Q78 were suppressed in *Fuz*^{-/-} HEK293 cells. The parental HEK293 cells were used as control. *n* = 3.
- C** Knockdown of *Fuz* expression suppressed JNK phosphorylation and caspase-3 cleavage in ATXN3tr-Q78-expressing rat primary cortical neurons. *n* = 3.
- D** Knockdown of *Fuz* expression suppressed the activation of JNK and caspase-3 in SCA3 patient fibroblasts. *n* = 3.
- E, F** (E) Knockdown of *fy* expression rescued neurodegenerative eye phenotype in SCA3 transgenic flies. The integrity of rhabdomeres in ATXN3fl-Q27 flies was not affected upon *fy* knockdown. The flies were of genotypes *w*; *gmr::Gal4* UAS::ATXN3fl-Q27/+; +/+; *w*; *gmr::Gal4* UAS::ATXN3fl-Q27/UAS::fy-dsRNA^{KK100638}; +/+; *w*; *gmr::Gal4* UAS::ATXN3fl-Q84/+ and *w*; *gmr::Gal4*/UAS::fy-dsRNA^{KK100638}; UAS::ATXN3fl-Q84/+. Scale bars: 5 μm. (F) is the quantification of (E). Error bars represent s.e.m., *n* = 3. For every control or experimental group, a total of 200 ommatidia collected from 20 fly eyes were examined in each replicate. Statistical analysis was performed using one-way ANOVA followed by *post hoc* Tukey's test. ******P* < 0.05, ********P* < 0.001.

Data information: Beta-tubulin was used as loading control. *n* represents the number of biological replicates. Only representative images and blots are shown.

Source data are available online for this figure.

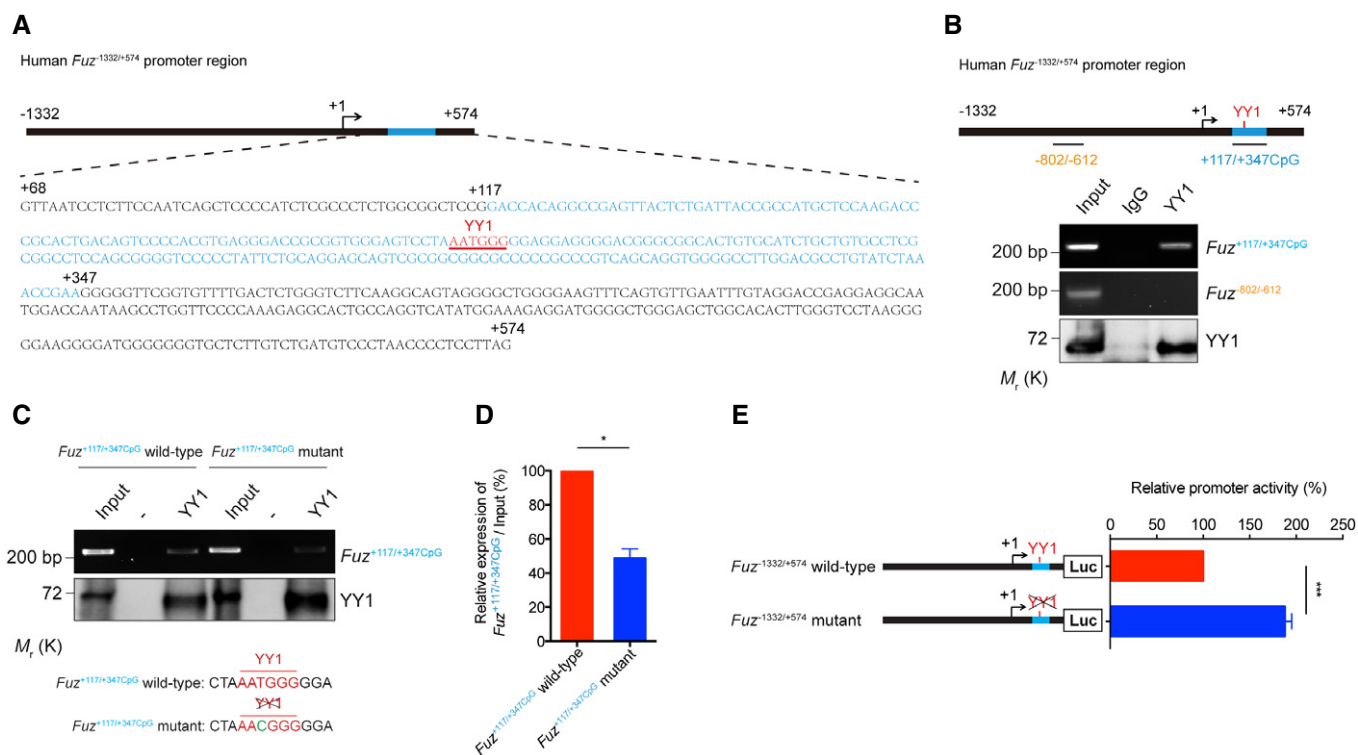


Figure 4. YY1 interacts with *Fuz* promoter *in vivo* and *in vitro*.

- A** Schematic representation of the human *Fuz*^{-1332/+574} promoter region. The *Fuz*^{+68/+574} was enlarged to show the detailed nucleotide sequence. A putative CpG island was found within *Fuz*^{+68/+574} and was defined as *Fuz*^{+117/+347CpG}. “+1” is the transcriptional initiation site (arrow). The CpG island is highlighted in blue, and sequence of the YY1 binding site is underlined and highlighted in red.
- B** Chromatin immunoprecipitation assay demonstrated the binding between YY1 protein and *Fuz*^{+117/+347CpG} DNA fragment. The blue bar indicates the *Fuz*^{+117/+347CpG} sequence. However, *Fuz*^{-802/-612} (orange) represents a region that did not show interaction with YY1 protein. *n* = 3.
- C, D** (C) *In vitro* DNA binding assay demonstrated the binding between purified YY1 protein and purified *Fuz*^{+117/+347CpG} DNA fragment. When a mutation (green) was introduced to the YY1 site (red) within the *Fuz*^{+117/+347CpG} fragment, YY1 binding was reduced. (D) is the quantification of the intensity of the *Fuz*^{+117/+347CpG} DNA bands as shown in (C). Error bars represent s.e.m., *n* = 3. Statistical analysis was performed using two-tailed unpaired Student's *t*-test. **P* < 0.05.
- E** Mutating the YY1 binding site in the *Fuz* promoter increased its transcriptional activity in HEK293 cells. Error bars represent s.e.m., *n* = 5. Statistical analysis was performed using two-tailed unpaired Student's *t*-test. ****P* < 0.001.

Data information: *n* represents the number of biological replicates. Only representative gels and blots are shown. Source data are available online for this figure.

whereas YY1 knockdown exerted an opposite effect (Fig 5E). These results strongly indicate that YY1 represses *Fuz* transcription via hypermethylating the *Fuz* promoter.

Expanded polyQ derepresses *Fuz* expression via perturbing the function of YY1

We sought to determine whether the changes in CpG island methylation in the *Fuz* promoter occur in cells expressing the polyQ disease protein ATXN3tr-Q78. Indeed, we found that the *Fuz*^{+117/+347CpG} was less methylated in ATXN3tr-Q78-expressing cells when compared with the ATXN3tr-Q27 or untransfected control (Fig 5F). Remarkably, the *Fuz*^{+117/+347CpG} hypomethylation status in the ATXN3tr-Q78-expressing cells was restored upon YY1 coexpression (Fig 5F), indicating that YY1 affects *Fuz* induction through altering its promoter DNA methylation. A similar effect was also observed in rat primary cortical neurons expressing ATXN3tr-Q78 (Fig EV3E). We further demonstrated that YY1 overexpression reduced *Fuz* protein expression, JNK phosphorylation and caspase-3

cleavage in both HEK293 cells and rat primary cortical neurons that expressed ATXN3tr-Q78 (Figs 5G and EV3F).

Recruitment of YY1 to protein aggregates and a reduction of its soluble level in polyQ diseases

We next evaluated YY1 protein expression in cerebellar cortex samples collected from SCA3 patients. When compared with age-matched control group, the SCA3 group exhibited reduced YY1 protein level (Fig 6A and B). Furthermore, we observed a similar reduction in SCA3 transgenic mouse brains (Fig 6C). Despite a change in YY1 protein level was detected, we found that YY1 mRNA expression was not altered in these mice (Fig 6C). An immunofluorescence analysis revealed that endogenous YY1 was recruited to polyQ protein aggregates in ATXN3-Q84-expressing cells (Fig 6D). This explains the reduction of soluble YY1 protein expression in the SCA3 models (Fig 6A–C).

We took a domain deletion mapping approach to determine which domains contribute to the recruitment of YY1 to polyQ protein

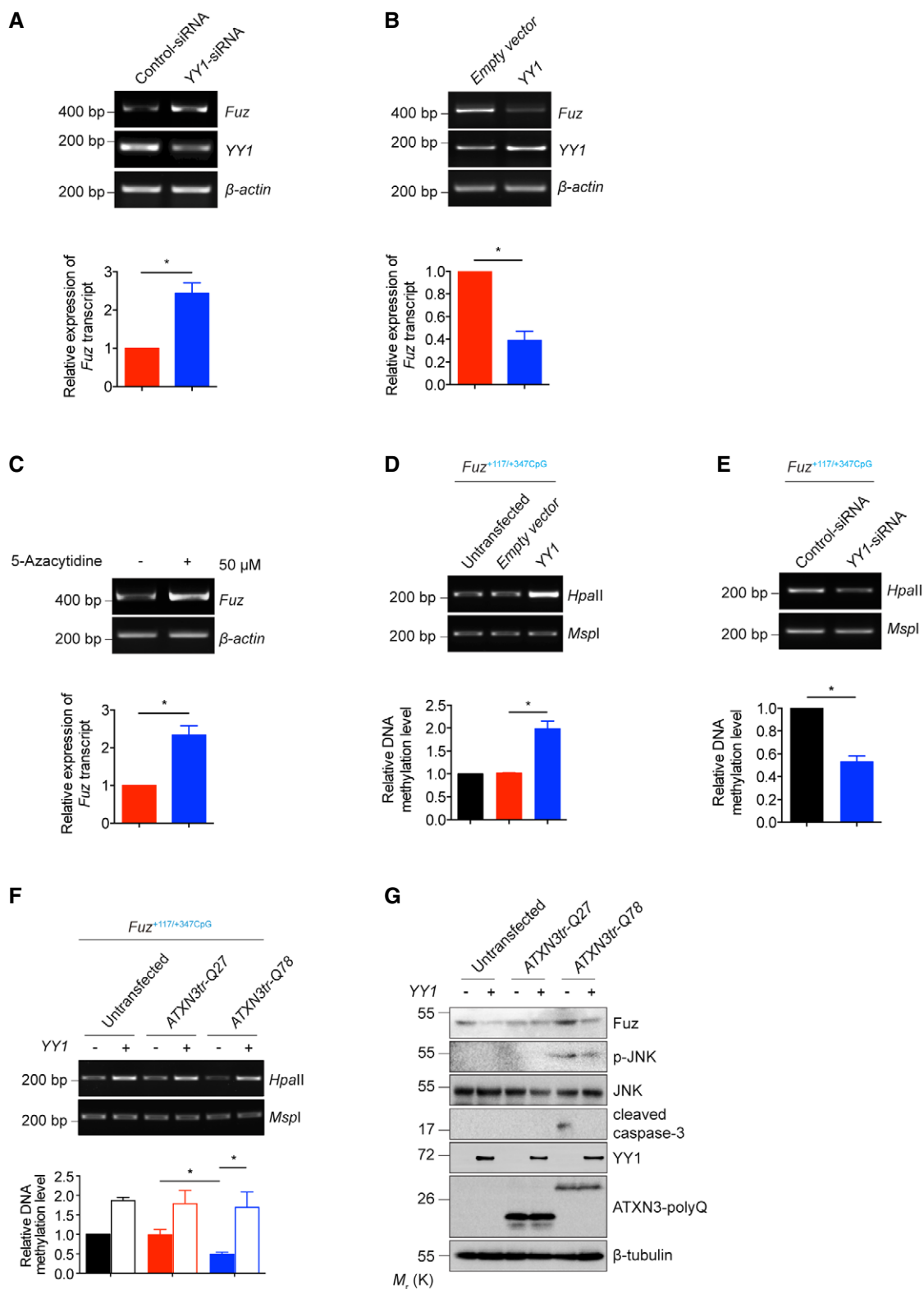


Figure 5.

aggregates (Fig 6E). The truncated YY1 proteins were independently coexpressed with ATXN3-Q84 in our SCA3 cell model; the colocalization of the truncated YY1 proteins with polyQ protein aggregates was

determined by confocal microscopy. Similar to the endogenous YY1 protein (Fig 6D), the YY1¹⁵⁴⁻⁴¹⁴ truncated protein was recruited to the polyQ protein aggregates. In contrast, the YY1²²⁷⁻⁴¹⁴ and

Figure 5. Expanded polyQ perturbs the function of YY1 to derepress Fuz expression.

- A Knockdown of YY1 expression upregulated *Fuz* expression in HEK293 cells. Lower panel shows the quantification of *Fuz* transcript expression relative to controls. Error bars represent s.e.m., $n = 3$. Statistical analysis was performed using two-tailed unpaired Student's *t*-test. $*P < 0.05$.
- B Overexpression of YY1 downregulated *Fuz* expression in HEK293 cells. Lower panel shows the quantification of *Fuz* transcript expression relative to controls. Error bars represent s.e.m., $n = 3$. Statistical analysis was performed using two-tailed unpaired Student's *t*-test. $*P < 0.05$.
- C 5-Azacytidine treatment induced the expression of *Fuz* in HEK293 cells. Lower panel shows the quantification of *Fuz* transcript expression relative to controls. Error bars represent s.e.m., $n = 3$. Statistical analysis was performed using two-tailed unpaired Student's *t*-test. $*P < 0.05$.
- D, E Overexpression of YY1 promoted the hypermethylation (D) while knockdown of YY1 expression led to the hypomethylation (E) of *Fuz*^{+117/+347CpG}. Lower panel shows the quantification of DNA methylation level of *Fuz*^{+117/+347CpG} relative to controls. Error bars represent s.e.m., $n = 3$. Statistical analysis was performed using two-tailed unpaired Student's *t*-test. $*P < 0.05$.
- F Overexpression of YY1 promoted the hypermethylation of *Fuz*^{+117/+347CpG} in the untransfected or ATXN3tr-Q27-expressing HEK293 cells. The ATXN3tr-Q78-mediated hypomethylation of *Fuz*^{+117/+347CpG} was rescued by YY1 overexpression. Lower panel shows the quantification of DNA methylation level of *Fuz*^{+117/+347CpG} relative to controls. Error bars represent s.e.m., $n = 3$. Statistical analysis was performed using one-way ANOVA followed by *post hoc* Tukey's test. $*P < 0.05$.
- G Overexpression of YY1 suppressed the ATXN3tr-Q78-mediated *Fuz* induction, JNK phosphorylation and caspase-3 cleavage in HEK293 cells. $n = 3$.
- Data information: *beta-actin* or *beta-tubulin* was used as loading control. n represents the number of biological replicates. Only representative gels and blots are shown. Source data are available online for this figure.

YY1^{AREPO} truncated proteins did not colocalize with polyQ protein aggregates (Fig 6F). The region that was deleted in both YY1^{227–414} and YY1^{AREPO} is the REcruitment of POlycomb (REPO) domain; our result thus indicates that the REPO domain is required for the recruitment of YY1 to polyQ protein aggregates.

In addition to YY1, the binding sites for two other neuronal transcriptional regulators nuclear receptor subfamily 3 group C member 1 (NR3C1; [35]) and Wilms tumour 1 (WT1; [36]) were predicted within *Fuz*^{+68/+574} promoter region (Fig EV4A). We investigated the protein expression and localization of both NR3C1 and WT1 in polyQ-expressing cells. In contrast to YY1 (Fig 6A), soluble protein levels of NR3C1 and WT1 in ATXN3tr-Q78-expressing cells were comparable to the controls (Fig EV4B). We also did not observe the recruitment of NR3C1 and WT1 to polyQ protein aggregates (Fig EV4C and D).

In addition to the toxic expanded polyQ protein, expanded CAG *polyQ* transcript also contributes to the polyQ disease pathogenesis [37]. When cells were transfected with *EGFP-CAG78* that only produces the expanded *polyQ* transcript but not the polyQ protein, the expression of *Fuz* remained unchanged when compared with the unexpanded control *EGFP-CAG27*. Both the *CAG27/78* sequences were inserted in the untranslated region of the *EGFP* DNA construct [38]. In contrast, when cells were transfected with the *ATXN3tr-CAA/G78* transgene which harbours a mixture of CAG and CAA glutamine codons in its polyQ-coding domain [39], *Fuz* induction was still detected (Fig EV4E). The *ATXN3tr-CAA/G78* construct possesses polyQ protein toxicity and exhibits diminished CAG RNA

toxicity. These results clearly demonstrate that the expanded polyQ protein, but not the expanded CAG *polyQ* transcript, triggers *Fuz*/*Fuz* induction.

Fuz/Fuz expression is upregulated in A β _{1–42}, Tau and α -synuclein models

In addition to polyQ diseases, we detected increased level of *Fuz* protein in rat primary cortical neurons treated with A β _{1–42} peptide and also neurons that were transfected with *Htttr-Q92*, *ATXN3tr-Q78*, *α -synuclein* or *Tau* construct (Fig 7A and Appendix Fig S2A). In contrast, no such induction was observed when neurons were treated with MPP⁺, a toxin that causes parkinsonism and triggers apoptotic cell death in mammals ([40]; Fig 7A and Appendix Fig S2B). Neither did we observe *Fuz* induction in neurons that had undergone oxidative stress nor heat-shock treatment (Fig 7A and Appendix Fig S2C and D). Consistent with neuronal cell findings, *Fuz*/*Fuz* induction was observed in A β _{1–42}-treated or *Tau*-/ *α -synuclein*-transfected HEK293 cells (Fig EV5A–C). These results suggest that *Fuz* induction is triggered by toxic disease peptide/proteins.

Fuz promoter sequence is hypomethylated in A β _{1–42}, Tau and α -synuclein models

By means of luciferase assay, we further demonstrated that the *Fuz*^{+68/+574} promoter region is responding to A β _{1–42} treatment

Figure 6. Soluble YY1 protein level is reduced in polyQ diseases.

- A, B (A) Soluble YY1 protein level was reduced in SCA3 patient brain samples versus age-matched controls. Background information on the control and patient brains are summarized in Appendix Tables S2 and S3. (B) is the quantification of (A). Error bars represent s.e.m., $n = 6$. Statistical analysis was performed using two-tailed unpaired Student's *t*-test. $***P < 0.01$.
- C Expression of soluble YY1 protein, but not YY1 transcript, was reduced in the brains of 6-month-old SCA3 transgenic mice. Lower panel shows the quantification of YY1 transcript and protein expression relative to controls. Error bars represent s.e.m., $n = 3$. Statistical analysis was performed using two-tailed unpaired Student's *t*-test. ns represents no significant difference. $*P < 0.05$.
- D YY1 protein was sequestered to the ATXN3-Q84 protein aggregates (green) in HEK293 cells, while its nuclear localization was not affected in ATXN3-Q28-expressing cells or cells with no ATXN3-Q84 protein aggregate detected. Endogenous YY1 (red) was stained with anti-YY1 antibody. Cell nuclei (blue) were stained with Hoechst 33342. Scale bars: 5 μ m. $n = 3$.
- E Schematic representation of the domain structure of the human full-length and truncated YY1 proteins used in this study.
- F YY1^{155–414}, but not YY1^{227–414} and YY1^{AREPO} proteins (red), was sequestered to the ATXN3-Q84 protein aggregates (green) in HEK293 cells. Cell nuclei (blue) were stained with Hoechst 33342. Scale bars: 5 μ m. $n = 3$.

Data information: *GAPDH* or *beta-tubulin* was used as loading control. n represents the number of biological replicates. Only representative images, gels and blots are shown. Source data are available online for this figure.

(Fig EV5D) and Tau expression (Fig EV5E). Next, we examined whether the methylation of $Fuz^{+117/+347CpG}$ was altered in $A\beta_{1-42}$ -treated or Tau-expressing cells. As shown in Fig 7B and C, the $Fuz^{+117/+347CpG}$ was found to be less methylated upon $A\beta_{1-42}$ treatment or *Tau* transfection. When YY1 was

coexpressed, methylation status of this region was restored (Fig 7B and C).

When we further analysed the *Fuz* promoter, we identified another region ($Fuz^{-2032/-1332}$) that is responsive to α -synuclein expression (Fig EV5F) and found a putative CpG island

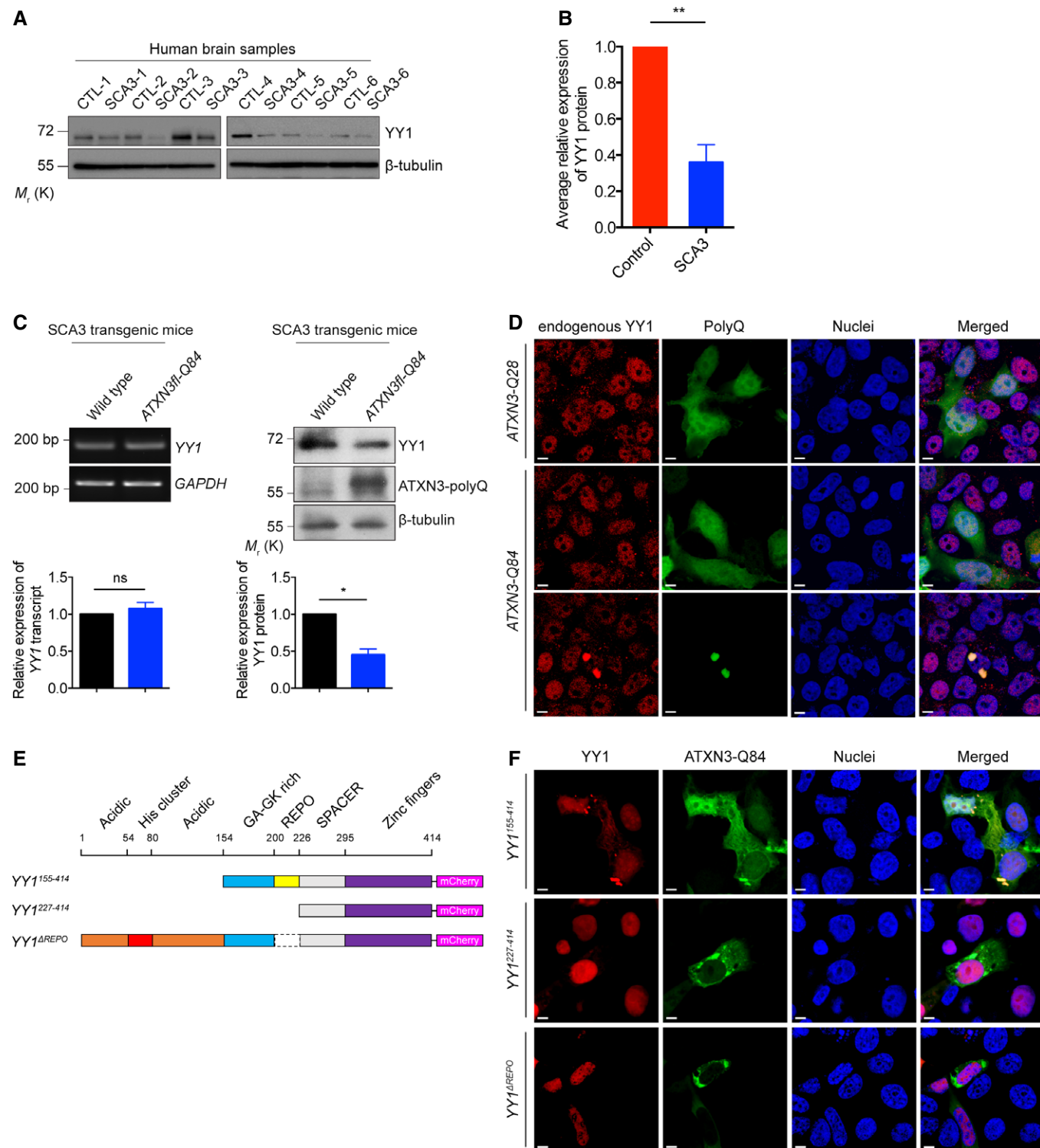


Figure 6.

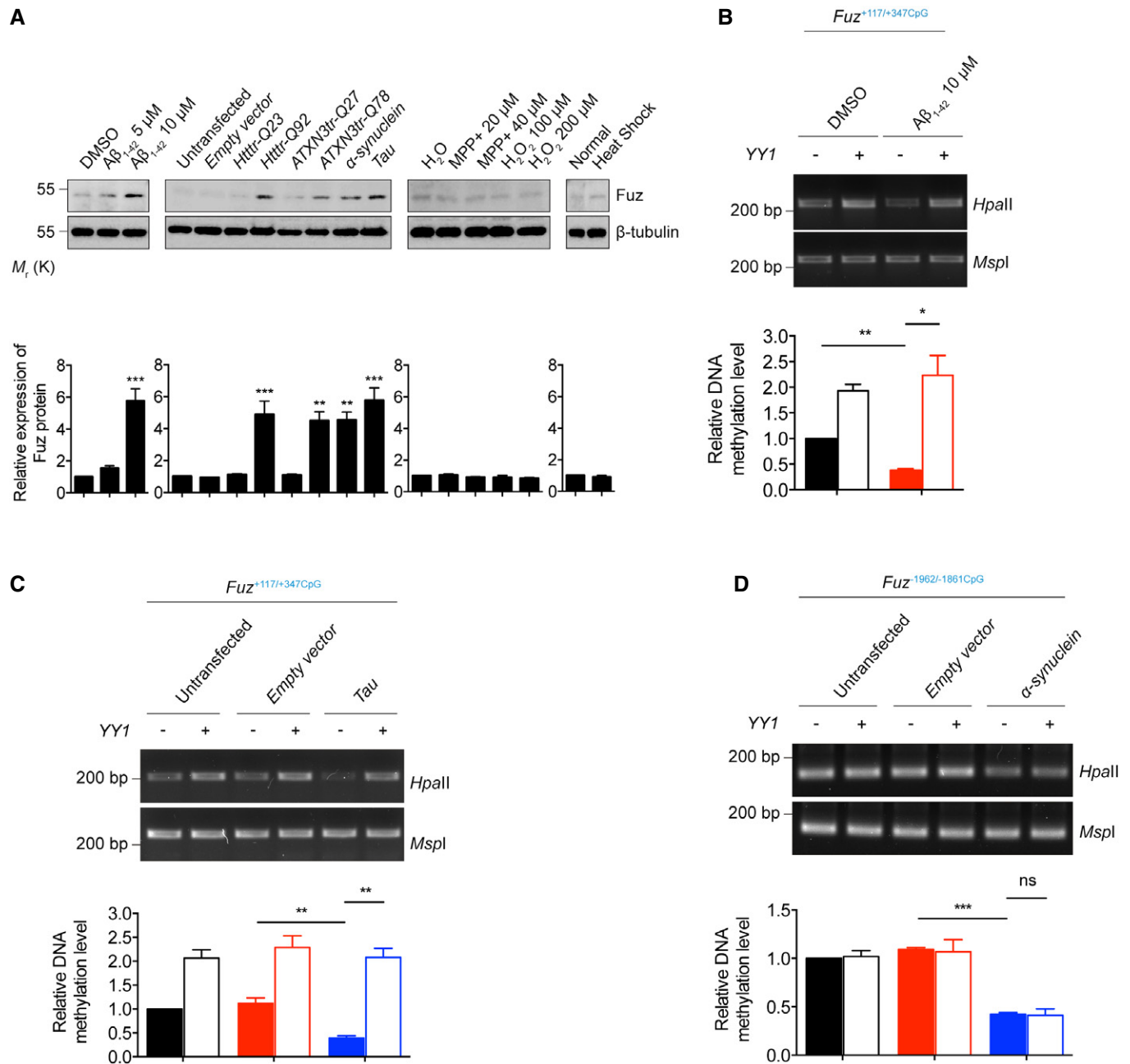


Figure 7. Fuz protein expression and its transcriptional regulation in different stress and neurodegenerative disease conditions.

- A** Rat primary cortical neurons treated with Aβ₁₋₄₂ peptide, or transfected with *Htttr-Q92*, *ATXN3tr-Q78*, *α-synuclein*, *Tau* constructs induced Fuz protein expression. Such induction was not observed in neurons treated with MPP+, H₂O₂ or heat shock. Lower panel shows the quantification of Fuz protein expression relative to controls. Error bars represent s.e.m., *n* = 3. Statistical analysis was performed using one-way ANOVA followed by *post hoc* Tukey's test. ***P* < 0.01, ****P* < 0.001.
- B** Overexpression of YY1 promoted the hypermethylation of *Fuz*^{+117/+347CpG} in the DMSO-treated HEK293 cells. Treatment of Aβ₁₋₄₂ caused hypomethylation of *Fuz*^{+117/+347CpG}, while such hypomethylation was restored by YY1 overexpression. Lower panel shows the quantification of DNA methylation level of *Fuz*^{+117/+347CpG} relative to controls. Error bars represent s.e.m., *n* = 3. Statistical analysis was performed using one-way ANOVA followed by *post hoc* Tukey's test. **P* < 0.05, ***P* < 0.01.
- C** Overexpression of YY1 promoted the hypermethylation of *Fuz*^{+117/+347CpG} in the untransfected or *empty vector*-transfected HEK293 cells. The Tau-mediated hypomethylation of *Fuz*^{+117/+347CpG} was rescued by YY1 overexpression. Lower panel shows the quantification of DNA methylation level of *Fuz*^{+117/+347CpG} relative to controls. Error bars represent s.e.m., *n* = 3. Statistical analysis was performed using one-way ANOVA followed by *post hoc* Tukey's test. ****P* < 0.01.
- D** Overexpression of YY1 did not change the methylation of *Fuz*^{-1962/-1861CpG} in the untransfected or *empty vector*-transfected HEK293 cells. The α-synuclein-mediated hypomethylation of *Fuz*^{-1962/-1861CpG} was not restored by YY1 overexpression. Lower panel shows the quantification of DNA methylation level of *Fuz*^{-1962/-1861CpG} relative to controls. Error bars represent s.e.m., *n* = 3. Statistical analysis was performed using one-way ANOVA followed by *post hoc* Tukey's test. ns represents no significant difference. ****P* < 0.001.

Data information: Beta-tubulin was used as loading control. *n* represents the number of biological replicates. Only representative gels and blots are shown. Source data are available online for this figure.

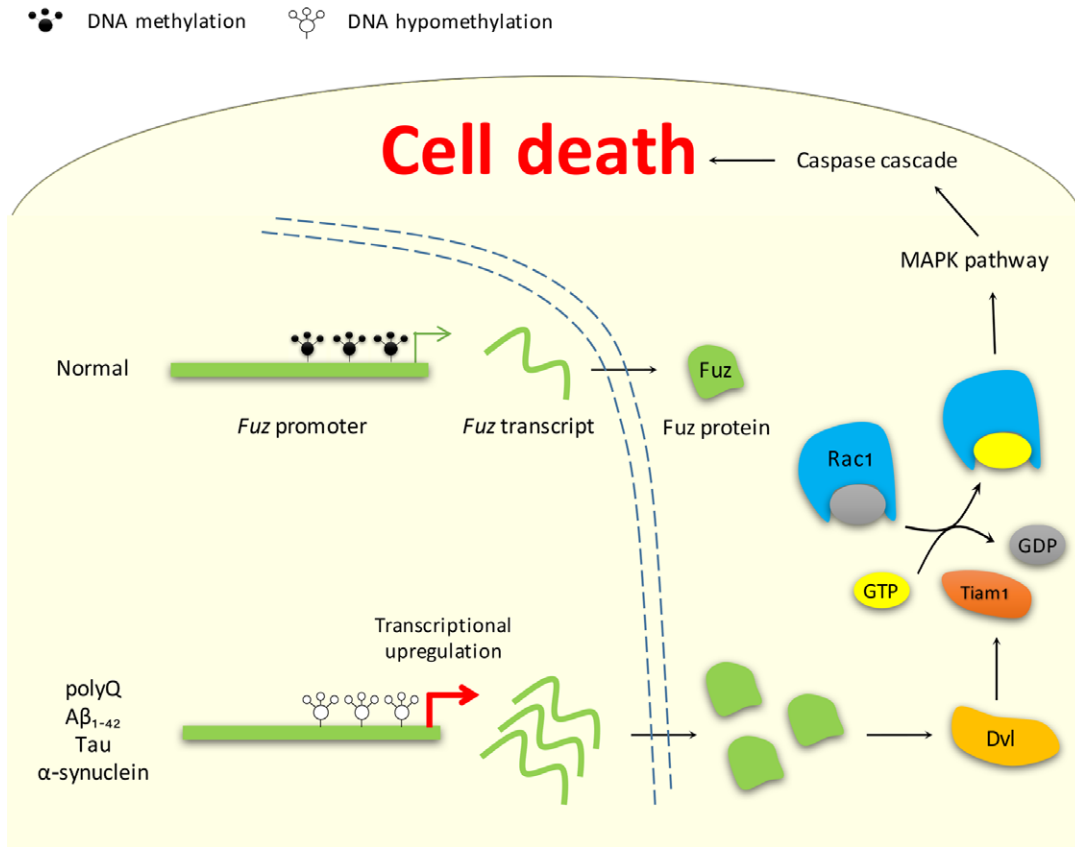


Figure 8. Model of Fuz-induced apoptosis in polyQ, A β ₁₋₄₂, Tau and α -synuclein models.

In normal condition, *Fuz* promoter is methylated. In polyQ, A β ₁₋₄₂, Tau and α -synuclein models, *Fuz* promoter is hypomethylated, and this results in transcriptional upregulation of *Fuz*. The accumulation of Fuz protein in turn stimulates the downstream Dvl/Rac1 GTPase/MEK1/JNK/caspase signalling pathway and induces neuronal cell death.

(*Fuz*^{-1962/-1861CpG}) within this region (Fig EV3D). We next sought to determine whether the methylation status of the *Fuz*^{-1962/-1861CpG} was affected by α -synuclein. As shown in Fig 7D, when α -synuclein was overexpressed, this region was found to be hypomethylated. However, no predicted YY1 binding site was predicted within the *Fuz*^{-1962/-1861CpG}. In line with the *in silico* prediction, YY1 overexpression did not alter the methylation status of *Fuz*^{-1962/-1861CpG} in α -synuclein-expressing cells (Fig 7D).

YY1 protein colocalizes with A β ₁₋₄₂ aggregates, but its localization is not changed in Tau and α -synuclein models

The A β ₁₋₄₂ peptide and Tau protein form aggregates [41,42] and cause dysregulation of gene expression [43,44]. We found that endogenous YY1 was recruited to A β ₁₋₄₂ aggregates (Fig EV5G). Our colocalization study further suggests that the N-terminal acidic and His cluster regions of YY1 play some roles in its sequestration to A β ₁₋₄₂ aggregates (Fig EV5G). In contrast, we did not observe recruitment of YY1 to Tau aggregates (Fig EV5H). Similarly, we also did not observe any change of YY1 localization pattern in α -synuclein-expressing cells (Fig EV5I). How *Fuz* transcriptional control is affected in Tau- and α -synuclein-mediated neurotoxicity warrants further investigation.

Discussion

This study unveiled a previously undescribed role of Fuz, a PCP effector, in the pathogenesis of multiple neurodegenerative diseases (Fig 8). We showed that Fuz, when overexpressed, triggers apoptosis in neuronal cells by activating the Dvl/Rac1 GTPase/MEK1/JNK/caspase signalling pathway (Fig 1A–K). Elevated level of *Fuz* expression was observed in cell models expressing Htttr-Q92 (Figs 7A and EV2A), ATXN3tr-Q78 (Figs 7A and EV2B), Tau (Figs 7A and EV5B), α -synuclein (Figs 7A and EV5C) or treated with A β ₁₋₄₂ peptide (Figs 7A and EV5A). Furthermore, our data demonstrate that *Fuz* promoter was hypomethylated in cells transfected with *ATXN3tr-Q78*, *α -synuclein*, and *Tau*, as well as A β ₁₋₄₂ peptide-treated cells (Figs 5F and 7B–D). All these conditions lead to the transcriptional upregulation of *Fuz* gene expression.

Tabler *et al* [45] observed the overproduction of neural crest cells in *Fuz*^{-/-} embryos and that *Fuz* mutant mice display excessive cell proliferation [21]. These findings highlight the role of Fuz in the regulation of cell survival and proliferation. Dishevelled is responsible for transducing Wnt signals to downstream pathways including PCP signalling [46]. Genetically, *Fuz* acts as a downstream effector of *Dvl* [3]. More recently, it was reported that Fuz could modulate the subcellular distribution of Dvl to regulate PCP [25], indicating

Fuz can regulate its downstream pathways via Dvl. In addition to the classical roles of Dvl and Fuz in PCP [1], our study discovered a previously undescribed function of Fuz in activating apoptotic signalling (Fig 1K). Fuz promotes the formation of Dvl “punctae” (Fig EV1E), which in turn triggers the Rac1 GTPase/MEKK1/JNK/caspase signalling axis to mediate apoptotic cell death (Fig 1A–K). Interestingly, knockdown of other PCP genes, including *Inturned*, *Fritz* and *Flamingo*, did not affect Fuz-induced caspase-3 cleavage (Fig EV1I–K). This strongly suggests that Fuz-induced apoptosis is independent of the PCP signalling pathway, but may specifically involve the pro-apoptotic functions of Dvl [47]. Since the regulation of apoptosis by Dvl involves the canonical Wnt signalling pathway [48], future investigations may examine the involvement of molecules such as GSK3 β and β -catenin in Fuz-induced apoptosis.

We previously reported that the downregulation of *pre-45S ribosomal RNA* expression in polyQ diseases can be caused by rDNA hypermethylation [38]. By contrast, here we observed that *Fuz* promoter is hypomethylated in polyQ diseases (Fig 5F). Furthermore, hypomethylation of the *Fuz* promoter was also observed in A β _{1–42} peptide-treated cells (Fig 7B), as well as in cells transfected with *Tau* (Fig 7C) and α -synuclein (Fig 7D), suggesting that *Fuz* hypomethylation may be a common pathogenic feature in multiple neurodegenerative diseases. Epigenetic regulation of gene transcription is reversible [49], and our findings highlight that targeted reversal of the pathologic epigenome would be a viable therapeutic strategy for treating neurodegenerative diseases in general.

Polyglutamine protein aggregation is a pathological hallmark of polyQ diseases [9]. Various cellular regulators, including transcriptional factors, are recruited to these aggregated macromolecular structures. Protein aggregates deplete the cellular activities of the sequestered cellular proteins and contribute to the neurotoxicity observed in polyQ diseases [50]. Alteration of cellular gene expression has widely been reported in polyQ diseases [51–53]. The sequestration of transcriptional factors to polyQ protein aggregates can downregulate the expression of cellular genes [54–56]. In this study, we are intrigued to have discovered a significant reduction of protein expression of a *Fuz* transcriptional repressor, YY1, in SCA3 patients (Fig 6A and B). We observed the recruitment of YY1 to polyQ protein aggregates in our SCA3 cell model (Fig 6D) and further demonstrated that the REPO domain is required for the recruitment of YY1 into polyQ protein aggregates (Fig 6F). The REPO domain is known for the recruitment of the polycomb group proteins into a multimeric protein complex required for transcriptional silencing [34]. When we examined whether the deletion of the REPO domain would disrupt YY1’s function in suppressing Fuz induction in SCA3 cell model, as expected we found that YY1^{AREPO} was less effective than full-length YY1 in suppressing the expanded polyQ-induced upregulation of Fuz (Fig EV4F). This indicates that the REPO domain is not only required for the recruitment of YY1 into polyQ protein aggregates, but it is also important for YY1 to suppress Fuz upregulation in polyQ diseases.

In addition to the suppression of Fuz upregulation, overexpression of YY1 also suppressed apoptosis in neurons expressing the expanded polyQ protein (Fig EV3F). A range of studies indicate that the function of YY1 is perturbed during neurodegeneration [57,58]. Our results unveil a new role of YY1 in polyQ pathogenesis, as demonstrated by the findings that deprivation of functional YY1 protein by expanded polyQ protein causes derepression of *Fuz*

transcription, followed by the induction of neuronal apoptosis. Moreover, we found that the *Fuz*^{+117/+347CpG} is responsive to multiple toxic protein insults, including expanded polyQ, A β _{1–42} and Tau (Appendix Table S1). In AD brains, YY1 protein was found to have undergone proteolytic cleavage, which results in the reduction of full-length YY1 protein level [59]. This is a plausible explanation to *Fuz* upregulation in A β _{1–42}-treated cells (Fig EV5A).

Our result indicates that the α -synuclein protein activates *Fuz* transcription via a different promoter region (*Fuz*^{–1962/–1861CpG}; Appendix Table S1). Although α -synuclein also induces *Fuz* promoter hypomethylation, it could not be restored by YY1 coexpression (Fig 7D), indicating other transcriptional regulatory factors may be involved. *In silico* analysis of this region identified a putative forkhead box A1 (FOXA1) transcriptional factor binding site in the *Fuz*^{–1962/–1861CpG}. FOXA1 has been implicated in the maintenance of dopaminergic neurons [60], and its expression also regulates the methylation of DNA sequences [61]. Further investigations would be needed to verify the involvement of FOXA1 in *Fuz* transcription regulation in α -synuclein-expressing cells.

In conclusion, our study shows that *Fuz* promoter is hypomethylated in expanded polyQ-, α -synuclein-, Tau-expressing and A β _{1–42}-treated cells. Instead of invoking the downregulation of pro-survival gene expression [62–64], we provide an alternative mechanistic explanation to how the transcriptional derepression of a pro-apoptotic gene can participate in the pathogenesis of neurodegenerative disorders.

Materials and Methods

Plasmids

The *pcDNA3.1-Tau-2N4R-V5/His* [65], *pcDNA3.1(+)-ATXN3tr-Q27/Q78* [66], *pcDNA3.1(+)-ATXN3tr-CAA/G78* [38], *pEGFP-CAG27/78* [38], *pCMV-Tag2B-Htttr-Q23/Q92* [67] and *pcDNA3.1(+)-Q19/Q81-EGFP-myc* constructs [66] were described previously. *pRK5-Rac1^{T17N}* was a gift from Gary Bokoch (Addgene plasmid # 12984). *pcDNA3.1(zeo)-Dvl* was a gift from Randall Moon (Addgene plasmid # 16758). *pmCherry-N1* was a gift from Michael Davidson (Addgene plasmid # 54517). *pEGFP-ATXN3-Q28/Q84* were gifts from Henry Paulson (Addgene plasmids # 22122 and 22123) [68]. *pCMV6-Inturned* (RC218556), *pCMV6-Fritz* (RC210824) and *pCMV6-Flamingo* (RC211860) were purchased from OriGene Technologies. *pGL4.17[luc2/Neo]* and *pTK-RL* were purchased from Promega. To generate the *pcDNA3.1(+)-flag- α -synuclein*, the α -synuclein DNA sequence was amplified from HEK293 cDNA template using primers *KpnI-flag- α -syn-F*, 5'-GGGGTACCATGGATTACAAGGACGATGACGATAA GATGGATGTATTCATGAAAGGAC-3' and *NotI- α -syn-R*, 5'-ATTTG CCGCCGCTTAGGCTTCAGGTTCTAGTGC-3'. The DNA fragment was subsequently subcloned into *pcDNA3.1(+)* vector (Thermo Fisher Scientific) using *KpnI* and *NotI*. To generate the *pcDNA3.1(+)-flag-Fuz*, the *Fuz* DNA sequence was amplified from HEK293 cDNA template using primers *EcoRI-flag-Fuz-F*, 5'-CCGGAATTCATG GATTACAAGGATGACGACGATAAAGATGGGGGAGGAGGGGAC-3' and *XhoI-Fuz-R*, 5'-CCGCTCGAGTCAAAGAAGTGGGGTGTAG-3'. The respective DNA fragments were then subcloned into *pcDNA3.1(+)* vector using *EcoRI* and *XhoI*. To generate the *pFuz-EGFP*, the *Fuz* DNA sequence was amplified from HEK293 cDNA template using

primers *EcoRI-Fuz-F*, 5'-CCGGAATTCATGGGGGAGGAGGGGAC-3' and *KpnI-Fuz-R*, 5'-CCGGTACCGTAAGAAGTGGGGTGAGG-3'. The resultant DNA fragments were subcloned into *pEGFP-N1* vector (Clontech Laboratories) using *EcoRI* and *KpnI*. To generate the *pcDNA3.1(+)-Human YY1-myc* and *pcDNA3.1(+)-Rat YY1-myc*, the human and rat *YY1* DNA sequences were amplified from HEK293 and rat primary cortical neuron cDNA templates, respectively. The primers used were *EcoRI-YY1-F*, 5'-CCGGAATTCATGGCCTCGGGC GACAC-3' and *XhoI-myc-YY1-R*, 5'-CCGCTCGAGTCACAGATCCTCT TCTGAGATGAGTTTTTCTGTTGTTTTTGGC-3'. The DNA fragments were subsequently subcloned into *pcDNA3.1(+)* vector using *EcoRI* and *XhoI*. To generate *YY1* deletion constructs, the *YY1¹⁵⁵⁻⁴¹⁴* and *YY1²²⁷⁻⁴¹⁴* DNA sequences were amplified from HEK293 cDNA template using primers *EcoRI-YY1-155-F*, 5'-CCGGAATTCATGGCGCCGCAAGAG-3'; *EcoRI-YY1-227-F*, 5'-CCGGAATTCATGGATGAAAAAAGATATTG-3'; and *KpnI-YY1-R*, 5'-CCGGTACCGTCTGGTTGTTTTTGGC-3'. The resultant DNA fragments were subcloned into *pmCherry-N1* vector using *EcoRI* and *KpnI* to generate the *pYY1¹⁵⁵⁻⁴¹⁴-mCherry* and *pYY1²²⁷⁻⁴¹⁴-mCherry*. Overlapping PCR method was used to generate the *YY1^{AREPO}* sequence, and the resultant DNA fragment was subcloned into *pmCherry-N1* vector using *EcoRI* and *KpnI* to generate the *pYY1^{AREPO}-mCherry*. Primers used for overlapping PCR were *EcoRI-YY1-F*, 5'-CCGGAATTCATGGCCTCGGGC GACAC-3'; *YY1^{AREPO}-R*, 5'-CTTTTTTTCATCGTTGCCCG-3'; *YY1^{AREPO}-F*, 5'-GGCGCCGAC GATGAAAAAAG-3'; and *KpnI-YY1-R*, 5'-CCGGTACCGTCTGGT TTTTTTGGC-3'. To generate *pcDNA3.1(+)-YY1^{AREPO}-myc*, the *YY1^{AREPO}* DNA sequence was amplified from *pYY1^{AREPO}-mCherry* using primers *EcoRI-YY1-F*, 5'-CCGGAATTCATGGCCTCGGGC GACAC-3' and *XhoI-myc-YY1-R*, 5'-CCGCTCGAGTCACAGATCCTCT TCTGAGATGAGTTTTTCTGTTGTTTTTGGC-3'. The resultant DNA fragment was subsequently subcloned into *pcDNA3.1(+)* vector using *EcoRI* and *XhoI*. The -2032 to +574, -1332 to +574 and +68 to +574 human *Fuz* promoter DNA sequences were amplified from HEK293 genomic DNA template using primers *NheI-Fuz Promoter -2032-F*, 5'-CCGCTAGCTTTGTTCTTGTGTTGCCAGGC-3'; *NheI-Fuz Promoter -1332-F*, 5'-CCGCTAGCGCACTTTGAGAGGCT GAGGT-3'; *NheI-Fuz Promoter +68-F*, 5'-CCGCTAGCGTTAATCC TCTTCCAATCAG-3' and *BglII-Fuz Promoter-R*, 5'-CCGAGATCTC TAAGGAGGGTTAGGG-3'. The resultant DNA fragments were subcloned into *pGL4.17[luc2/Neo]* luciferase vector using *NheI* and *BglII* to generate the *pGL4.17-Fuz^{-2032/+574}*, *pGL4.17-Fuz^{-1332/+574}* and *pGL4.17-Fuz^{+68/+574}*. Overlapping PCR method was used to generate the *Fuz promoter -1332/+574 YY1 mutant* sequence, and the resultant DNA fragment was subcloned into *pGL4.17[luc2/Neo]* luciferase vector using *NheI* and *BglII* to generate the *pGL4.17-Fuz^{-1332/+574} YY1 mutant*. Primers used for overlapping PCR were *NheI-Fuz Promoter -1332-F*, 5'-CCGGTACCGCACTTTGA GAGGCTGAGGT-3'; *YY1 mutant-F*, 5'-GAGTCTAAACGGGG GAGGAG-3'; *YY1 mutant-R*, 5'-CTCCTCCCCGTTTAGGACTC-3'; and *BglII-Fuz Promoter-R*, 5'-CCGAGATCTTAAGGAGGGTTAGGG-3'.

Cell cultures and transfection

The SCA3 patient fibroblasts (GM06151) [69] were obtained from the NIGMS Human Genetic Cell Repository at the Coriell Institute for Medical Research. The unaffected control fibroblasts (AG04351) [38] were obtained from the NIA Aging Cell Culture

Repository at the Coriell Institute for Medical Research. The *Fuz^{-/-}* HEK293 cell line was generated by GenScript using the CRISPR/Cas9 gene editing system. The targeting guide RNA sequence used was 5'-ACTGACCAATATCCGCAACG-3'. The mutant *Fuz* locus was PCR-amplified from the CRISPR-targeted cell clones and sequenced. The resultant *Fuz^{-/-}* clones were confirmed to carry a homozygous 1-bp insertion mutation in the coding region of endogenous *Fuz* locus. This insertion introduces a premature stop codon after the Arg 171 position. Both the HEK293 (Thermo Fisher Scientific) and fibroblasts were cultured using DMEM (GE Healthcare BioSciences) supplemented with 10% foetal bovine serum and 1% penicillin-streptomycin. The cells were maintained in a 37°C humidified cell culture incubator supplemented with 5% CO₂. Lipofectamine 2000 (Thermo Fisher Scientific) and Lipofectamine RNAiMAX (Thermo Fisher Scientific) were used in plasmid and siRNA transfection, respectively. For gene knockdown experiments, all ON-TARGETplus SMARTpool siRNAs were purchased from GE Healthcare BioSciences. In this study, 40 pmol of *MEKK1*-siRNA (L-003575-00-0005), 20 pmol of *Tiam1*-siRNA (L-003932-00-0005), 20 pmol of *Dvl*-siRNA (L-004070-00-0005), 20 pmol of *Inturned*-siRNA (L-031873-01-0005), 40 pmol of *Fritz*-siRNA (L-020947-02-0005), 40 pmol of *Flamingo*-siRNA (L-005460-00-0005), 20 pmol of human *Fuz*-siRNA (L-016342-02-0005), 60 pmol of rat *Fuz*-siRNA (L-082437-02-0005) and 5 pmol of *YY1*-siRNA (L-011796-00-0005) were used to knockdown the respective gene expression. Non-targeting siRNA (D-001210-01-50) was used as control. Rat primary cortical neurons were isolated and cultured as previously reported [70]. Neurons were incubated with 3 µg of plasmids or 60 pmol of siRNAs in primary neuron transfection reagent (VVP-1003, Lonza). Neurons were transfected using Amaxa Nucleofection system (Lonza) according to the manufacturer's instructions. The SCA3 patient fibroblasts (GM06153) [71] were obtained from the NIGMS Human Genetic Cell Repository at the Coriell Institute for Medical Research. The SCA3 fibroblasts and unaffected control fibroblasts (AG04351) were reprogrammed with the Yamanaka factors, Oct3/4, Sox2, Klf4 and c-Myc using the Sendai virus delivery system. The reprogramming protocol was performed according to manufacturer's instructions (CytoTune®-iPS 2.0 Sendai Reprogramming kit, Thermo Fisher Scientific). Induced pluripotent stem cells (iPSCs) at passage 12 were further induced to neural progenitor cells using the STEMdiff™ Neural Induction Medium (STEMCELL Technologies, Inc.). Induced neural progenitor cells (iNPCs) were maintained in STEMdiff™ Neural Progenitor Medium (STEMCELL Technologies, Inc.) and used for experiments at passage 4. For the characterization of iNPC cells, RNAs were extracted from cells, followed by quantitative PCR to determine the expression of *Nestin*. The primers used were *Nestin-F*, 5'-GTCTCAGGACAGTGCTGAGCCTTC-3' and *Nestin-R*, 5'-TCCCC TGAGGACCAGGAGTCTC-3'.

Drosophila stocks

All fly crosses were set up in a 21.5°C incubator. Fly lines *UAS::ATXN3fl-Q27/Q84* [27], *gmr::Gal4* [72] and *UAS::Httexon1-Q93* [73] were described previously. The *UAS::fy-dsRNA* line (KK100638) was obtained from Vienna *Drosophila* RNAi Center, and the *fy³* line (8875) [3] was obtained from Bloomington *Drosophila* Stock Center.

Mouse strain

The SCA3 transgenic mouse strain B6;CBA-Tg(ATXN3*)84.2Cce/IbezJ [74] (012705) was obtained from The Jackson Laboratory. Genotyping was performed using the genomic DNA isolated from tail biopsy. Primers used for genotyping were *Mouse MJD-F*, 5'-ACAATGACACGATGTTGGCT-3'; *Mouse MJD-R*, 5'-AAACAAA TATTCGCCAGGTGTAG-3'; *Mouse GAPDH-F*, 5'-ACATCATCCCTG CATCCACTG-3'; and *Mouse GAPDH-R*, 5'-ACAACCTGGTCCTC AGTGT-3'. Whole-brain samples were collected from homozygous SCA3 transgenic mice at 6 months of age. All animal procedures were conducted with the approval of the Animal Experimentation Ethics Committee of The Chinese University of Hong Kong.

Human brain samples

Brain tissues from five SCA3 patients were obtained from the NIH NeuroBioBank at the University of Maryland, Baltimore, MD. Brain tissues from one SCA3 case and six age-matched controls were obtained through the New York Brain Bank, Columbia University, New York, NY. Background information including age, gender and post-mortem interval of controls and SCA3 cases are listed in Appendix Tables S2 and S3. Brain tissues were homogenized in SDS sample buffer (100 mM Tris-HCl pH 6.8, 2% SDS, 20% glycerol). Protein concentration was determined using Bradford Protein Assay Kit (Thermo Fisher Scientific). The homogenate was heated at 99°C for 10 min. A total of 60 µg of each sample was used for immunoblotting.

Human TissueScan cDNA arrays

Human brain tissue cDNA array (HBRT301, OriGene Technologies) and human normal tissue cDNA array (HMRT304, OriGene Technologies) were used to determine the expression profile of *Fuz* in humans. The qPCR was performed using an ABI 7500 real-time PCR system. The following TaqMan probes were used *Fuz* (Assay ID: Hs01547302_m1), *beta-actin* (Assay ID: Hs99999903_m1). Relative expression of *Fuz* was normalized against *beta-actin* using the $2^{-\Delta CT}$ method.

RNA isolation and RT-PCR

TRIzol reagent (Thermo Fisher Scientific) was used to extract RNA from mammalian cells, adult fly heads and mouse brains. Two micrograms of RNA was used for reverse transcription using the ImProm-II™ Reverse Transcription System (Promega) according to the manufacturer's instructions. Primers used in this study were *Human Fuz-F*, 5'-CCGGAATTCATGCCCTTCACACAGACATC-3'; *Human Fuz-R*, 5'-CCGGTACCGTTCAAAGAAGTGGGGTGAGG-3'; *YY1-F*, 5'-TCAGATTCTCATCCCGTGC-3'; *YY1-R*, 5'-ACTCTTCTT GCCGCTCTTCT-3'; *Actin-F*, 5'-ATGTGCAAGCCGGTTTCGC-3'; *Actin-R*, 5'-CGACACGACGCTCATTGTAG-3'; *Drosophila fuzzy-F*, 5'-CATATGCCATGAGTGCCTAC-3'; *Drosophila fuzzy-R*, 5'-TATTAG CATGGATCGGTTGC-3'; *Drosophila ATXN3-polyQ-F*, 5'-CGCGGATC CAAAACAGCAGCAAAAGC-3'; *Drosophila ATXN3-polyQ-R*, 5'-CGCACCGGTTCTGTCTCTGATAGGTCC-3'; *Mouse Fuz-F*, 5'-CCCG TCAACAGCTTCTTTC-3'; and *Mouse Fuz-R*, 5'-CCAGGAAGCTGTC GATGAGA-3'.

Chromatin immunoprecipitation assay

Cells were fixed with 1% formaldehyde for 10 min at 37°C. Ice-cold 1× PBS was used to wash cells twice. Binding buffer (10 mM HEPES, pH 7.5, 10% glycerol, 5 mM MgCl₂, 142.5 mM KCl, 1 mM EDTA, 1% Triton X-100) supplemented with protease inhibitor cocktail (Sigma-Aldrich) was then added to the samples. Sonication was applied to lyse the cells (Duty Cycle 30, Output Control 3, Timer 30 s, Sonifier 450, Branson Ultrasonics), and the samples were incubated at 4°C for 1 h with rotation. The samples were centrifuged at 4°C for 30 min at 14,000 × g. A fraction of the supernatant was saved as "Input". The dynabeads protein G (10004D, Thermo Fisher Scientific), together with anti-YY1 antibody (ab109237, Abcam), was quickly added to the remaining samples, and the mixture was incubated at 4°C overnight with gentle rotation. The subsequent washing and elution procedures were performed according to the manufacturer's instructions (ChIP Assay Kit, Merck Millipore). The recovered genomic DNA was analysed by PCR using the primers *Fuz -802-F*, 5'-TTGTCACATCCATAAAATAG-3'; *Fuz -612-R*, 5'-TACCATGTAAAATGTGAAAATC-3'; *Fuz +117-F*, 5'-GACCACAGG CCGAGTTACTC-3'; and *Fuz +347-R*, 5'-TTCGGTTTAGATACAGG CGTC-3'.

In vitro DNA binding assay

In vitro DNA binding assay was performed as previously described [75]. In brief, *Fuz* promoter-containing DNA fragments were PCR-amplified from *pGL4.17-Fuz -1332/+574* and *pGL4.17-Fuz -1332/+574 YY1 mutant* constructs, respectively. The primers used were *Fuz +117-F*, 5'-GACCACAGGCCGAGTTACTC-3' and *Fuz +347-R*, 5'-TTCGGTTTAGATACAGGCCGTC-3'. Five nanograms of wild-type and YY1 mutant DNAs was independently mixed with 400 ng of YY1 protein (ab187479, Abcam), 0.4 µg of anti-YY1 antibody (ab109237, Abcam) and 40 µl of dynabeads protein G (10004D, Thermo Fisher Scientific) in 500 µl binding buffer (10 mM HEPES, pH 7.5, 10% glycerol, 5 mM MgCl₂, 142.5 mM KCl, 1 mM EDTA, 1% Triton X-100). The mixture was incubated at 4°C overnight with gentle rotation. Prior to elution, the protein/DNA mixture was washed with binding buffer for five times. The recovered genomic DNA was analysed by PCR using the primers *Fuz +117-F*, 5'-GACCACAGGCCGAGTTACTC-3' and *Fuz +347-R*, 5'-TTCGGTTTAGATACAGGCCGTC-3'.

Protein sample preparation, immunoblot analysis and antibodies used in this study

Proteins were extracted from HEK293 cells or rat primary cortical neurons using SDS sample buffer. For protein extraction from mice, half of the brain was homogenized in protein lysis buffer (50 mM Tris-HCl, pH 7.6, 150 mM NaCl, 10% NP-40, 5% sodium deoxycholate). All protein samples were boiled at 99°C for 10 min, prior to immunoblot analysis. Primary antibodies used were anti-cleaved caspase-3 (9664, 1:500), anti-p-JNK (9251, 1:500), anti-JNK (9252, 1:1,000), anti-myc (2276, 1:2,000) from Cell Signaling Technology; anti-p-MEKK1 (ab138662, 1:1,000), anti-MEKK1 (ab69533, 1:1,000), anti-Fuz (ab111842, 1:500), anti-WT1 (ab89901, 1:1,000), anti-Flamingo (ab90817, 1:500), anti-YY1 (ab109237, 1:1,000), anti-beta-tubulin (ab6046, 1:2,000) from Abcam; anti-Tiam1 (sc-393315, 1:100), anti-dishevelled (sc-8027, 1:200), anti-NR3C1 (sc-56851,

1:500) from Santa Cruz Biotechnology; anti-Inturned (LS-C169884-50, 1:500) from LifeSpan BioSciences; anti-Fritz (PA524271, 1:500) from Thermo Fisher Scientific; anti-ATXN3 (MAB5360, 1:500) from Merck Millipore; anti-polyglutamine (P1874, 1:1,000), anti-flag (F3165, 1:500), anti-HA (H3663, 1:500) and anti-His (27-4710-01, 1:1,000) from Sigma-Aldrich; anti-Hsp70 (SPA-812C, 1:1,000) from Enzo Life Sciences. Secondary antibodies used for immunoblot analyses were goat anti-rabbit (11-035-045, 1:5,000) and goat anti-mouse (115-035-062, 1:10,000) from Jackson ImmunoResearch.

Co-immunoprecipitation assay

Cells were washed once with ice-cold 1× PBS. Binding buffer (10 mM HEPES, pH 7.5, 10% glycerol, 5 mM MgCl₂, 142.5 mM KCl, 1 mM EDTA, 1% Triton X-100) supplemented with protease inhibitor cocktail (Sigma-Aldrich) was then added to the samples. Sonication was applied to lyse the cells (duty cycle 30, output control 3, timer 30 s, Sonifier 450, Branson Ultrasonics), and the samples were incubated at 4°C for 1 h with rotation. The samples were centrifuged at 4°C for 20 min at 14,000 × g. A fraction of the supernatant was saved as “Input”. The dynabeads protein G (10004D, Thermo Fisher Scientific), together with anti-flag antibody (2368, Cell Signaling Technology) was quickly added to the remaining samples, and the mixture was incubated at 4°C overnight with gentle rotation. On the following day, the beads were washed for three times with binding buffer and then resuspended in SDS sample buffer. All protein samples were boiled at 99°C for 10 min, prior to immunoblot analysis. The Dvl and flag-Fuz were detected using anti-Dvl (sc-8027, Santa Cruz Biotechnology) and anti-flag (F3165, Sigma-Aldrich) antibodies, respectively.

Drug and peptide treatments

Pan-caspase inhibitor Z-VAD-FMK (Enzo Life Sciences) was used at 20 μM, and the treatment lasted for 48 h. The JNK inhibitor SP600125 (Merck Millipore) was used at 10, 30 or 50 μM, and the treatment lasted for 24 h. The DNA methyltransferase inhibitor 5-azacytidine (Sigma-Aldrich) was used at 50 μM, and the treatment lasted for 8 h. The MPP⁺ (Sigma-Aldrich) was used at 20 or 40 μM, and the treatment lasted for 48 h. The H₂O₂ (Merck Millipore) was used at 100 or 200 μM, and the treatment lasted for 48 h. The Aβ₁₋₄₂ was pre-incubated at 37°C for 1 h before used at 5 or 10 μM, and the treatment lasted for 24 h. The fluorescently labelled Aβ₁₋₄₂ (AS-60479-01, AnaSpec) was prepared as previously described [76]. The working concentration was 2 μM, and the treatment lasted for 24 h.

Heat-shock treatment

Heat shock was performed by placing the rat primary cortical neurons at 42°C for 2 h. The neurons were then recovered at 37°C for 24 h.

Lactate dehydrogenase (LDH) assay

For HEK293 cells, LDH assay was performed 72 h post-transfection. For rat primary cortical neurons, LDH assay was performed 96 h post-transfection. The procedures were performed according to manufacturer's instructions (CytoTox 96 Non-Radioactive Cytotoxicity Assay Kit, Promega).

Terminal Deoxynucleotidyl Transferase dUTP Nick End Labelling (TUNEL) assay

Forty-eight hours post-transfection, HEK293 cells were fixed with 1% paraformaldehyde. The remaining procedures were performed according to manufacturer's instructions (APO-BrdU™ TUNEL Assay Kit, Thermo Fisher Scientific). Cell images were acquired on an Olympus IX-81 FV1000 confocal microscope (Olympus) using a 20× objective lens and Olympus Fluoview software (version 4.2a).

Rac1 activation assay

For the Rac1 activation assay, HEK293 cells were harvested 24 h post-transfection. The subsequent procedures were performed according to the manufacturer's instructions (RhoA/Rac1/Cdc42 Activation Assay Combo Kit, Cell Biolabs).

Luciferase assay

Cell culture medium was removed 24 h post-transfection, and the following procedures were performed according to the manufacturer's instructions (Dual-Glo Luciferase Assay Kit, Promega). The firefly and *Renilla* luminescence were detected using a luminometer (Tecan). The relative luciferase activity was determined by calculating the ratio between firefly and *Renilla* luminescence.

HpaII DNA methylation assay

HpaII DNA methylation assay was performed as previously described [38]. The primers used were *Fuz* +117-F, 5'-GACCA CAGGCCGAGTTACTC-3'; *Fuz* +347-R, 5'-TTCGGTTAGATA CAGCGTC-3'; *Fuz* -1962-F, 5'-TTCAACGGATTATCCTGC-3'; *Fuz* -1861-R, 5'-GAGAAACCCCGCTCTAC-3'; *Rat Fuz* +50-F, 5'-TCCAAACAGCAGGCCACTTTC-3'; and *Rat Fuz* +312-R, 5'-GCATG TATGCAGTCCCAGCTTC-3'.

Immunocytochemistry

The HEK293 cells were seeded on cover slip (Marienfeld-Superior). Cells were fixed with 3.7% paraformaldehyde. The primary and secondary antibodies used were anti-NR3C1 (1:200; sc-56851, Santa Cruz Biotechnology), anti-WT1 (1:400; ab89901, Abcam), anti-YY1 antibody (1:400; ab109237, Abcam), anti-flag (1:200; F3165, Sigma-Aldrich), anti-His antibody (1:200; 27-4710-01, Sigma-Aldrich), goat anti-mouse IgG (H+L) FITC conjugate (1:400; Zymed), goat anti-mouse IgG (H+L) Cy3 conjugate (1:400; Zymed) and goat anti-rabbit IgG (H+L) Cy3 conjugate (1:400; Zymed), respectively. The cell nuclei were stained with Hoechst 33342 (1:400; Thermo Fisher Scientific). Cell images were acquired on an Olympus IX-81 FV1000 confocal microscope (Olympus) using a 63× water immersion objective lens and Olympus Fluoview software (version 4.2a). For the iNPC characterization, the primary and secondary antibodies used were anti-Nestin antibody (1:200; sc-1703, Santa Cruz Biotechnology) and goat anti-mouse IgG (H+L) Cy3 conjugate (1:400; Zymed), respectively. The cell nuclei were stained with Hoechst 33342 (1:400; Thermo Fisher Scientific). Cell images were acquired on an Olympus IX-81 FV1000 confocal microscope (Olympus) using a 20× objective lens and Olympus Fluoview software (version 4.2a). Ten

micromolar of CM-H₂DCFDA (Thermo Fisher Scientific) was added to H₂O₂-treated rat primary cortical neurons to monitor reactive oxygen species (ROS) production, and ROS was detected after a 30-min incubation at 37°C. The images were acquired on an Olympus IX-81 FV1000 confocal microscope (Olympus) using a 20× objective lens and Olympus Fluoview software (version 4.2a).

Pseudopupil assay

Pseudopupil assay was performed as previously described [77]. The images of ommatidia were captured by a SPOT Insight CCD camera (Diagnostic Instruments Inc.), and all images were processed using the SPOT Advanced software (version 5.2; Diagnostic Instruments, Inc.) and Adobe Photoshop 7.0 software. For each control or experimental group, a total of 200 ommatidia collected from 20 fly eyes were examined. The average number of rhabdomeres from each ommatidia was used to determine ommatidial integrity.

Statistical analyses

The two-tailed, unpaired Student's *t*-test and one-way ANOVA followed by *post hoc* Tukey's test were applied to determine the difference between each group. *, ** and *** represent $P < 0.05$, $P < 0.01$ and $P < 0.001$, respectively, which are considered statistically significant.

Data and software availability

Fuz and *fuzzy* promoter sequences are deposited in GenBank under the accession numbers NG_032843 and NT_033779.5. The intensity of the protein or DNA bands were quantified using the ImageJ software (<https://imagej.nih.gov/ij/>) [78]. Transcription factor binding sites were predicted using the ConSite (<http://consite.genereg.net/>) [79], Transcription factor affinity prediction (http://trap.molgen.mpg.de/cgi-bin/trap_form.cgi) [80] and PROMO (http://algggen.lsi.upc.es/cgi-bin/promo_v3/promo/promoi nit.cgi?dirDB=TF_8.3) [81] softwares. The CpG islands were predicted using the MethPrimer (<http://www.urogene.org/meth primer/>) [82] software.

Expanded View for this article is available online.

Acknowledgements

We thank former and present members of the Laboratory of *Drosophila* Research for insightful comments and discussion. We are grateful to Dr. S.H. Kuo and Dr. P.L. Faust from Columbia University for providing human brain samples. Human SCA3 tissue was obtained from the NIH Neurobiobank at the University of Maryland. Control brain tissue and one SCA3 case were obtained from the New York Brain Bank, Columbia University. Control and SCA3 iPSCs were generated by Dr. J.J. Kim from the Human Stem Cell Core at Baylor College of Medicine. This work was supported by the General Research Fund (14100714) of the Hong Kong Research Grants Council; CUHK Vice-Chancellor's One-Off Discretionary Fund (VCF2014011); CUHK One-off Funding for Joint Lab/Research Collaboration (3132980); CUHK Faculty of Science Strategic Development Fund (FACULTY-P17173); CUHK Gerald Choa Neuroscience Centre (7105306); and donations from Chow Tai Fook Charity Foundation (6903898) and Hong Kong Spinocerebellar Ataxia Association (6903291).

Author contributions

ZSC and HVEC planned the study and designed the experiments. ZSC, FMC, LL, XL, WL, SP, and QZ carried out the experiments and analyses. YA, ZSC, HVEC, T-FC, ACK, KMK, K-FL, JCKN, and WTW interpreted the results. ZSC, ACK, and HVEC wrote the manuscript.

Conflict of interest

The authors declare that they have no conflict of interest.

References

- Butler MT, Wallingford JB (2017) Planar cell polarity in development and disease. *Nat Rev Mol Cell Biol* 18: 375–388
- Axelrod JD, Miller JR, Shulman JM, Moon RT, Perrimon N (1998) Differential recruitment of dishevelled provides signaling specificity in the planar cell polarity and wingless signaling pathways. *Genes Dev* 12: 2610–2622
- Collier S, Gubb D (1997) *Drosophila* tissue polarity requires the cell-autonomous activity of the fuzzy gene, which encodes a novel transmembrane protein. *Development* 124: 4029–4037
- Devenport D (2014) The cell biology of planar cell polarity. *J Cell Biol* 207: 171–179
- Ohata S, Nakatani J, Herranz-Perez V, Cheng J, Belinson H, Inubushi T, Snider WD, Garcia-Verdugo JM, Wynshaw-Boris A, Alvarez-Buylla A (2014) Loss of dishevelleds disrupts planar polarity in ependymal motile cilia and results in hydrocephalus. *Neuron* 83: 558–571
- Gray RS, Abitua PB, Wlodarczyk BJ, Szabo-Rogers HL, Blanchard O, Lee I, Weiss GS, Liu KJ, Marcotte EM, Wallingford JB *et al* (2009) The planar cell polarity effector Fuz is essential for targeted membrane trafficking, cilio-genesis and mouse embryonic development. *Nat Cell Biol* 11: 1225–1232
- Seo JH, Zilber Y, Babayeva S, Liu J, Kyriakopoulos P, De Marco P, Merello E, Capra V, Gros P, Torban E (2011) Mutations in the planar cell polarity gene, Fuzzy, are associated with neural tube defects in humans. *Hum Mol Genet* 20: 4324–4333
- Adegbuyiro A, Sedighi F, Pilkington IV AW, Groover S, Legleiter J (2017) Proteins containing expanded polyglutamine tracts and neurodegenerative disease. *Biochemistry* 56: 1199–1217
- Kuiper EF, de Mattos EP, Jardim LB, Kampinga HH, Bergink S (2017) Chaperones in polyglutamine aggregation: beyond the Q-stretch. *Front Neurosci* 11: 145
- Orr HT, Zoghbi HY (2007) Trinucleotide repeat disorders. *Annu Rev Neurosci* 30: 575–621
- Fan HC, Ho LI, Chi CS, Chen SJ, Peng GS, Chan TM, Lin SZ, Harn HJ (2014) Polyglutamine (PolyQ) diseases: genetics to treatments. *Cell Transplant* 23: 441–458
- Everett CM, Wood NW (2004) Trinucleotide repeats and neurodegenerative disease. *Brain* 127: 2385–2405
- Elmore S (2007) Apoptosis: a review of programmed cell death. *Toxicol Pathol* 35: 495–516
- Chatterjee A, Saha S, Chakraborty A, Silva-Fernandes A, Mandal SM, Neves-Carvalho A, Liu Y, Pandita RK, Hegde ML, Hegde PM *et al* (2015) The role of the mammalian DNA end-processing enzyme polynucleotide kinase 3'-phosphatase in spinocerebellar ataxia type 3 pathogenesis. *PLoS Genet* 11: e1004749
- Liu H, Li X, Ning G, Zhu S, Ma X, Liu X, Liu C, Huang M, Schmitt I, Wullner U *et al* (2016) The Machado-Joseph disease deubiquitinase ataxin-3 regulates the stability and apoptotic function of p53. *PLoS Biol* 14: e2000733

16. Hart MP, Gitler AD (2012) ALS-associated ataxin 2 polyQ expansions enhance stress-induced caspase 3 activation and increase TDP-43 pathological modifications. *J Neurosci* 32: 9133–9142
17. Ueda M, Li S, Itoh M, Hayakawa-Yano Y, Wang MX, Hayakawa M, Hasebe-Matsubara R, Ohta K, Ohta E, Mizuno A et al (2014) Polyglutamine expansion disturbs the endoplasmic reticulum formation, leading to caspase-7 activation through Bax. *Biochem Biophys Res Commun* 443: 1232–1238
18. Sanchez I, Xu CJ, Juo P, Kakizaka A, Blenis J, Yuan J (1999) Caspase-8 is required for cell death induced by expanded polyglutamine repeats. *Neuron* 22: 623–633
19. Ghavami S, Shojaei S, Yeganeh B, Ande SR, Jangamreddy JR, Mehrpour M, Christoffersson J, Chaabane W, Moghadam AR, Kashani HH et al (2014) Autophagy and apoptosis dysfunction in neurodegenerative disorders. *Prog Neurobiol* 112: 24–49
20. Andorfer C, Acker CM, Kress Y, Hof PR, Duff K, Davies P (2005) Cell-cycle reentry and cell death in transgenic mice expressing nonmutant human tau isoforms. *J Neurosci* 25: 5446–5454
21. Zhang Z, Wlodarczyk BJ, Niederreither K, Venugopalan S, Florez S, Finnell RH, Amendt BA (2011) Fuz regulates craniofacial development through tissue specific responses to signaling factors. *PLoS One* 6: e24608
22. Lu H, Ning X, Tao X, Ren J, Song X, Tao W, Zhu L, Han L, Tao T, Yang J (2016) MEK1 associated with neuronal apoptosis following intracerebral hemorrhage. *Neurochem Res* 41: 3308–3321
23. Bos JL, Rehmann H, Wittinghofer A (2007) GEFs and GAPs: critical elements in the control of small G proteins. *Cell* 129: 865–877
24. Toliaas KF, Bikoff JB, Burette A, Paradis S, Harrar D, Tavazoie S, Weinberg RJ, Greenberg ME (2005) The Rac1-GEF Tiam1 couples the NMDA receptor to the activity-dependent development of dendritic arbors and spines. *Neuron* 45: 525–538
25. Zilber Y, Babayeva S, Seo JH, Liu JJ, Mootin S, Torban E (2013) The PCP effector Fuzzy controls cilia assembly and signaling by recruiting Rab8 and dishevelled to the primary cilium. *Mol Biol Cell* 24: 555–565
26. Cajanek L, Ganji RS, Henriques-Oliveira C, Theofilopoulos S, Konik P, Bryja V, Arenas E (2013) Tiam1 regulates the Wnt/Dvl/Rac1 signaling pathway and the differentiation of midbrain dopaminergic neurons. *Mol Cell Biol* 33: 59–70
27. Warrick JM, Morabito LM, Bilen J, Gordesky-Gold B, Faust LZ, Paulson HL, Bonini NM (2005) Ataxin-3 suppresses polyglutamine neurodegeneration in *Drosophila* by a ubiquitin-associated mechanism. *Mol Cell* 18: 37–48
28. Shi Y, Seto E, Chang LS, Shenk T (1991) Transcriptional repression by YY1, a human GLI-Kruppel-related protein, and relief of repression by adenovirus E1A protein. *Cell* 67: 377–388
29. He Y, Casaccia-Bonnel P (2008) The Yin and Yang of YY1 in the nervous system. *J Neurochem* 106: 1493–1502
30. Fritsch C, Brown JL, Kassis JA, Muller J (1999) The DNA-binding polycomb group protein pleiohomeotic mediates silencing of a *Drosophila* homeotic gene. *Development* 126: 3905–3913
31. Atchison L, Ghias A, Wilkinson F, Bonini N, Atchison ML (2003) Transcription factor YY1 functions as a PcG protein *in vivo*. *EMBO J* 22: 1347–1358
32. He Y, Kim JY, Dupree J, Tewari A, Melendez-Vasquez C, Svaren J, Casaccia P (2010) Yy1 as a molecular link between neuregulin and transcriptional modulation of peripheral myelination. *Nat Neurosci* 13: 1472–1480
33. Hwang SS, Jang SW, Kim MK, Kim LK, Kim BS, Kim HS, Kim K, Lee W, Flavell RA, Lee GR (2016) YY1 inhibits differentiation and function of regulatory T cells by blocking Foxp3 expression and activity. *Nat Commun* 7: 10789
34. Ko CY, Hsu HC, Shen MR, Chang WC, Wang JM (2008) Epigenetic silencing of CCAAT/enhancer-binding protein delta activity by YY1/polycomb group/DNA methyltransferase complex. *J Biol Chem* 283: 30919–30932
35. Tronche F, Kellendonk C, Kretz O, Gass P, Anlag K, Orban PC, Bock R, Klein R, Schutz G (1999) Disruption of the glucocorticoid receptor gene in the nervous system results in reduced anxiety. *Nat Genet* 23: 99–103
36. Wagner KD, Wagner N, Vidal VP, Schley G, Wilhelm D, Schedl A, Englert C, Scholz H (2002) The Wilms' tumor gene Wt1 is required for normal development of the retina. *EMBO J* 21: 1398–1405
37. Li LB, Yu Z, Teng X, Bonini NM (2008) RNA toxicity is a component of ataxin-3 degeneration in *Drosophila*. *Nature* 453: 1107–1111
38. Tsoi H, Lau TC, Tsang SY, Lau KF, Chan HY (2012) CAG expansion induces nucleolar stress in polyglutamine diseases. *Proc Natl Acad Sci USA* 109: 13428–13433
39. Tsoi H, Lau CK, Lau KF, Chan HY (2011) Perturbation of U2AF65/NXF1-mediated RNA nuclear export enhances RNA toxicity in polyQ diseases. *Hum Mol Genet* 20: 3787–3797
40. Venderova K, Park DS (2012) Programmed cell death in Parkinson's disease. *Cold Spring Harb Perspect Med* 2: a009365
41. Goedert M, Spillantini MG (2017) Propagation of Tau aggregates. *Mol Brain* 10: 18
42. Esbjorner EK, Chan F, Rees E, Erdelyi M, Luheshi LM, Bertocchini CW, Kaminski CF, Dobson CM, Kaminski Schierle GS (2014) Direct observations of amyloid beta self-assembly in live cells provide insights into differences in the kinetics of Abeta(1-40) and Abeta(1-42) aggregation. *Chem Biol* 21: 732–742
43. Allaman I, Gavillet M, Belanger M, Laroche T, Viertl D, Lashuel HA, Magistretti PJ (2010) Amyloid-beta aggregates cause alterations of astrocytic metabolic phenotype: impact on neuronal viability. *J Neurosci* 30: 3326–3338
44. Frost B, Hemberg M, Lewis J, Feany MB (2014) Tau promotes neurodegeneration through global chromatin relaxation. *Nat Neurosci* 17: 357–366
45. Tabler JM, Barrell WB, Szabo-Rogers HL, Healy C, Yeung Y, Perdiguero EG, Schulz C, Yannakoudakis BZ, Mesbahi A, Wlodarczyk B et al (2013) Fuz mutant mice reveal shared mechanisms between ciliopathies and FGF-related syndromes. *Dev Cell* 25: 623–635
46. Shimizu N, Ishitani S, Sato A, Shibuya H, Ishitani T (2014) Hipk2 and PP1c cooperate to maintain Dvl protein levels required for Wnt signal transduction. *Cell Rep* 8: 1391–1404
47. Strovel ET, Sussman DJ (1999) Transient overexpression of murine dishevelled genes results in apoptotic cell death. *Exp Cell Res* 253: 637–648
48. van Gijn ME, Snel F, Cleutjens JP, Smits JF, Blankesteijn WM (2001) Overexpression of components of the Frizzled-Dishevelled cascade results in apoptotic cell death, mediated by beta-catenin. *Exp Cell Res* 265: 46–53
49. Qin L, Dong Z, Zhang JT (2014) Reversible epigenetic regulation of 14-3-3sigma expression in acquired gemcitabine resistance by uhrf1 and DNA methyltransferase 1. *Mol Pharmacol* 86: 561–569
50. Mohan RD, Abmayr SM, Workman JL (2014) The expanding role for chromatin and transcription in polyglutamine disease. *Curr Opin Genet Dev* 26: 96–104
51. Yu-Taeger L, Bonin M, Stricker-Shaver J, Riess O, Nguyen HH (2017) Dysregulation of gene expression in the striatum of BACHD rats

- expressing full-length mutant huntingtin and associated abnormalities on molecular and protein levels. *Neuropharmacology* 117: 260–272
52. Huen NY, Wong SL, Chan HY (2007) Transcriptional malfunctioning of heat shock protein gene expression in spinocerebellar ataxias. *Cerebellum* 6: 111–117
 53. Huen NY, Chan HY (2005) Dynamic regulation of molecular chaperone gene expression in polyglutamine disease. *Biochem Biophys Res Commun* 334: 1074–1084
 54. Yamanaka T, Miyazaki H, Oyama F, Kurosawa M, Washizu C, Doi H, Nukina N (2008) Mutant Huntingtin reduces HSP70 expression through the sequestration of NF-Y transcription factor. *EMBO J* 27: 827–839
 55. Nucifora Jr FC, Sasaki M, Peters MF, Huang H, Cooper JK, Yamada M, Takahashi H, Tsuji S, Troncoso J, Dawson VL et al (2001) Interference by huntingtin and atrophin-1 with cbp-mediated transcription leading to cellular toxicity. *Science* 291: 2423–2428
 56. Steffan JS, Kazantsev A, Spasic-Boskovic O, Greenwald M, Zhu YZ, Gohler H, Wanker EE, Bates GP, Housman DE, Thompson LM (2000) The Huntington's disease protein interacts with p53 and CREB-binding protein and represses transcription. *Proc Natl Acad Sci USA* 97: 6763–6768
 57. Rosas S, Vargas MA, Lopez-Bayghen E, Ortega A (2007) Glutamate-dependent transcriptional regulation of GLAST/EAAT1: a role for YY1. *J Neurochem* 101: 1134–1144
 58. Lee SG, Kim K, Kegelman TP, Dash R, Das SK, Choi JK, Emdad L, Howlett EL, Jeon HY, Su ZZ et al (2011) Oncogene AEG-1 promotes glioma-induced neurodegeneration by increasing glutamate excitotoxicity. *Cancer Res* 71: 6514–6523
 59. Aubry S, Shin W, Cray JF, Lefort R, Qureshi YH, Lefebvre C, Califano A, Shelanski ML (2015) Assembly and interrogation of Alzheimer's disease genetic networks reveal novel regulators of progression. *PLoS One* 10: e0120352
 60. Domanskyi A, Alter H, Vogt MA, Gass P, Vinnikov IA (2014) Transcription factors Foxa1 and Foxa2 are required for adult dopamine neurons maintenance. *Front Cell Neurosci* 8: 275
 61. Serandour AA, Avner S, Percevault F, Demay F, Bizot M, Lucchetti-Miganeh C, Barloy-Hubler F, Brown M, Lupien M, Metivier R et al (2011) Epigenetic switch involved in activation of pioneer factor FOXA1-dependent enhancers. *Genome Res* 21: 555–565
 62. Pugazhenti S, Wang M, Pham S, Sze CI, Eckman CB (2011) Downregulation of CREB expression in Alzheimer's brain and in Aβ-treated rat hippocampal neurons. *Mol Neurodegener* 6: 60
 63. Motyl J, Wencil PL, Cieslik M, Strosznajder RP, Strosznajder JB (2017) Alpha-synuclein alters differently gene expression of Sirts, PARPs and other stress response proteins: implications for neurodegenerative disorders. *Mol Neurobiol* 55: 727–740
 64. Saavedra A, Garcia-Martinez JM, Xifro X, Giral A, Torres-Peraza JF, Canals JM, Diaz-Hernandez M, Lucas JJ, Alberch J, Perez-Navarro E (2010) PH domain leucine-rich repeat protein phosphatase 1 contributes to maintain the activation of the PI3K/Akt pro-survival pathway in Huntington's disease striatum. *Cell Death Differ* 17: 324–335
 65. Lee CW, Lau KF, Miller CC, Shaw PC (2003) Glycogen synthase kinase-3 beta-mediated tau phosphorylation in cultured cell lines. *NeuroReport* 14: 257–260
 66. Chan WM, Tsoi H, Wu CC, Wong CH, Cheng TC, Li HY, Lau KF, Shaw PC, Perrimon N, Chan HY (2011) Expanded polyglutamine domain possesses nuclear export activity which modulates subcellular localization and toxicity of polyQ disease protein via exportin-1. *Hum Mol Genet* 20: 1738–1750
 67. Chow WN, Luk HW, Chan HY, Lau KF (2012) Degradation of mutant huntingtin via the ubiquitin/proteasome system is modulated by FE65. *Biochem J* 443: 681–689
 68. Chai Y, Shao J, Miller VM, Williams A, Paulson HL (2002) Live-cell imaging reveals divergent intracellular dynamics of polyglutamine disease proteins and supports a sequestration model of pathogenesis. *Proc Natl Acad Sci USA* 99: 9310–9315
 69. Evers MM, Pepers BA, van Deutekom JC, Mulders SA, den Dunnen JT, Aartsma-Rus A, van Ommen GJ, van Roon-Mom WM (2011) Targeting several CAG expansion diseases by a single antisense oligonucleotide. *PLoS One* 6: e24308
 70. Lau KF, Chan WM, Perkinson MS, Tudor EL, Chang RC, Chan HY, McLoughlin DM, Miller CC (2008) Dexas1 interacts with FE65 to regulate FE65-amyloid precursor protein-dependent transcription. *J Biol Chem* 283: 34728–34737
 71. Fiszer A, Mykowska A, Krzyzosiak WJ (2011) Inhibition of mutant huntingtin expression by RNA duplex targeting expanded CAG repeats. *Nucleic Acids Res* 39: 5578–5585
 72. Ellis MC, O'Neill EM, Rubin GM (1993) Expression of *Drosophila* glass protein and evidence for negative regulation of its activity in non-neuronal cells by another DNA-binding protein. *Development* 119: 855–865
 73. Steffan JS, Bodai L, Pallos J, Poelman M, McCampbell A, Apostol BL, Kazantsev A, Schmidt E, Zhu YZ, Greenwald M et al (2001) Histone deacetylase inhibitors arrest polyglutamine-dependent neurodegeneration in *Drosophila*. *Nature* 413: 739–743
 74. Cemal CK, Carroll CJ, Lawrence L, Lowrie MB, Ruddle P, Al-Mahdawi S, King RH, Pook MA, Huxley C, Chamberlain S (2002) YAC transgenic mice carrying pathological alleles of the MJD1 locus exhibit a mild and slowly progressive cerebellar deficit. *Hum Mol Genet* 11: 1075–1094
 75. Lee YL, Li YC, Su CH, Chiao CH, Lin IH, Hsu MT (2015) MAF1 represses CDKN1A through a Pol III-dependent mechanism. *Elife* 4: e06283
 76. Li W, Tang Y, Fan Z, Meng Y, Yang G, Luo J, Ke ZJ (2013) Autophagy is involved in oligodendroglial precursor-mediated clearance of amyloid peptide. *Mol Neurodegener* 8: 27
 77. Wong SL, Chan WM, Chan HY (2008) Sodium dodecyl sulfate-insoluble oligomers are involved in polyglutamine degeneration. *FASEB J* 22: 3348–3357
 78. Schneider CA, Rasband WS, Eliceiri KW (2012) NIH Image to ImageJ: 25 years of image analysis. *Nat Methods* 9: 671–675
 79. Sandelin A, Wasserman WW, Lenhard B (2004) ConSite: web-based prediction of regulatory elements using cross-species comparison. *Nucleic Acids Res* 32: W249–W252
 80. Roeder HG, Kanhere A, Manke T, Vingron M (2007) Predicting transcription factor affinities to DNA from a biophysical model. *Bioinformatics* 23: 134–141
 81. Messeguer X, Escudero R, Farre D, Nunez O, Martinez J, Alba MM (2002) PROMO: detection of known transcription regulatory elements using species-tailored searches. *Bioinformatics* 18: 333–334
 82. Li LC, Dahiya R (2002) MethPrimer: designing primers for methylation PCRs. *Bioinformatics* 18: 1427–1431